UNIVERSITY OF HELSINKI REPORT SERIES IN PHYSICS

HU-P-D166

Growth and modification of cluster-assembled thin films

Kristoffer Meinander

Division of Materials Physics
Department of Physics
Faculty of Science
University of Helsinki
Helsinki, Finland

ACADEMIC DISSERTATION

To be presented, with the permission of the Faculty of Science of the University of Helsinki, for public criticism in the Small Auditorium E204 of the Department of Physical Sciences (Physicum), on August 14th, 2009, at 12 o'clock p.m.

HELSINKI 2009

ISBN 978-952-10-5631-4 (printed version)
ISSN 0356-0961
Helsinki 2009
Helsinki University Printing House (Yliopistopaino)

ISBN 978-952-10-5632-1 (PDF version)
http://ethesis.helsinki.fi/
Helsinki 2009
Electronic Publications @ University of Helsinki (Helsingin yliopiston verkkojulkaisut)

Kristoffer Meinander **Growth and modification of cluster-assembled thin films**, University of Helsinki, 2009, 62 p.+appendices, University of Helsinki Report Series in Physics, HU-P-D166, ISSN 0356-0961, ISBN 978-952-10-5631-4 (printed version), ISBN 978-952-10-5632-1 (PDF version)

Classification (INSPEC): A6146, A6855, A6865, A8116
Keywords (INSPEC): cluster deposition, epitaxy, thin films, nanostructured materials, ion irradiation, densification, molecular dynamics, atomic force microscopy, self-assembly

ABSTRACT

Thin film applications have become increasingly important in our search for multifunctional and economically viable technological solutions of the future. Thin film coatings can be used for a multitude of purposes, ranging from a basic enhancement of aesthetic attributes to the addition of a complex surface functionality. Anything from electronic or optical properties, to an increased catalytic or biological activity, can be added or enhanced by the deposition of a thin film, with a thickness of only a few atomic layers at the best, on an already existing surface. Thin films offer both a means of saving in materials and the possibility for improving properties without a critical enlargement of devices.

Nanocluster deposition is a promising new method for the growth of structured thin films. Nanoclusters are small aggregates of atoms or molecules, ranging in sizes from only a few nanometers up to several hundreds of nanometers in diameter. Due to their large surface to volume ratio, and the confinement of atoms and electrons in all three dimensions, nanoclusters exhibit a wide variety of exotic properties that differ notably from those of both single atoms and bulk materials. Nanoclusters are a completely new type of building block for thin film deposition. As preformed entities, clusters provide a new means of tailoring the properties of thin films before their growth, simply by changing the size or composition of the clusters that are to be deposited. Contrary to contemporary methods of thin film growth, which mainly rely on the deposition of single atoms, cluster deposition also allows for a more precise assembly of thin films, as the configuration of single atoms with respect to each other is already predetermined in clusters.

Nanocluster deposition offers a possibility for the coating of virtually any material with a nanostructured thin film, and therein the enhancement of already existing physical or chemical properties, or the addition of some exciting new feature. A clearer understanding of cluster-surface interactions, and the growth of thin films by cluster deposition, must, however, be achieved, if clusters are to be successfully used in thin film technologies. Using a combination of experimental techniques and molecular dynamics simulations, both the deposition of nanoclusters, and the growth and modification of cluster-assembled thin films, are studied in this thesis. Emphasis is laid on an understanding of the interaction between metal clusters and surfaces, and therein the behaviour of these clusters during deposition and thin film growth.

The behaviour of single metal clusters, as they impact on clean metal surfaces, is analysed in detail, from which it is shown that there exists a cluster size and deposition energy dependent limit, below which epitaxial alignment occurs. If larger clusters are deposited at low energies, or cluster-surface interactions are weaker, non-epitaxial deposition will take place, resulting in the formation of nanocrystalline structures. The effect of cluster size and deposition energy on the morphology of cluster-assembled thin films is also determined, from which it is shown that nanocrystalline cluster-assembled films will be porous. Modification of these thin films, with the purpose of enhancing their mechanical properties and durability, without destroying their nanostructure, is presented. Irradiation with heavy ions is introduced as a feasible method for increasing the density, and therein the mechanical stability, of cluster-assembled thin films, without critically destroying their nanocrystalline properties.

The results of this thesis demonstrate that nanocluster deposition is a suitable technique for the growth of nanostructured thin films. The interactions between nanoclusters and their supporting surfaces must, however, be carefully considered, if a controlled growth of cluster-assembled thin films, with precisely tailored properties, is to be achieved.

Contents

1 INTRODUCTION

Ever since the concept of nano-scale phenomena was introduced by Richard P. Feynman in 1959 [1], there has been an ever increasing interest in the nano-scale world. With the development of novel experimental techniques, and the ability to successfully manipulate single atoms, gained in the early 1980s [2], the race towards the nano-scale has continued more frantic than ever. Crowds of scientists, and economists alike, all battle for the honour and benefit of new nano-discoveries, and eagerly propagate their faith in the achievements of this new science. A large part of this new field of *nanoscience* concerns the study of small particles called *nanoclusters* [3].

Nanoclusters themselves, small aggregates of atoms, with sizes ranging from a 1 – 100 nm, are not nearly as new as the science in which they are studied. Many brilliant works of art, originating from medieval days or earlier, relied on the exotic properties of nanoclusters to accentuate their luster. Some of the most alluring glazes of ancient Rome and Mesopotamia [4], and the brilliant colours of the Mayans [5], draw their enchanting secrets from the properties of embedded nanoclusters. One of the ancient world's more valuable artifacts, the Lycurgus cup, a glass chalice that appears green, when light is reflected off it, and red, when light is shown through it, is the fortuitous fruit of an accidental cluster production [6, 7].

Although clusters have existed for a very long time, as they even appear naturally in the world around us, only recently have they been studied by the scientific world. Insight into the size-controlled production of these atomic agglomerates [8–11], coupled together with the ability to manipulate them and study their properties, has opened up the possibility for their controlled use in applications [12]. Clusters exhibit novel properties, both physically and chemically [13], due to the confinement of atoms and electrons in all three dimensions, as their mechanical, electronic, optical, and even thermal behaviour is very much different from that of bulk materials. Large-scale manufacturing of nanocluster containing devices, is, however, still out of reach, as further insight into the production and behaviour of clusters is needed.

Studies presented in this thesis concern the deposition of nanoclusters, and their use in thin film growth. Thin films, if tailored correctly, can be used to cover almost any other material, either enhancing already existing properties, or introducing new properties, such as chemical reactivity or optical activity. If the exotic properties of nanoclusters could be incorporated into thin films, a completely new world of applications would be opened [14, 15]. The successful use of nanoclusters in thin film growth, coupled with the ability to retain the properties of free clusters within these films, however, requires a precise understanding of the interactions between clusters and supporting materials [16].

When nanoclusters are deposited on surfaces, in both physical and chemical deposition techniques, they will interact with these surfaces, resulting in a possible change of their properties. Depending on both deposition parameters, such as cluster size, kinetic energy, and temperature, and properties of the surface itself, different outcomes are possible. Both experimental and theoretical methods are required, if a clear understanding of deposition events is to be achieved. Using a combination of experimental cluster deposition, coupled with nano-scale analysis methods, and molecular dynamics simulations, the mechanisms of cluster-surface interactions, as well as the properties of cluster-assembled thin films, can be studied in detail. Results from these, show whether the use of nanoclusters in the growth of nanostructured thin films, will be possible within our conceivable future.

2 PURPOSE AND STRUCTURE OF THIS STUDY

The purpose of this thesis is to improve our understanding of cluster-surface interactions, during the physical deposition of clusters, and the mechanisms of growth and final properties of cluster-assembled thin films. These results aid in the development of cluster deposition technologies and further the search for novel thin film growth methods.

This thesis consists of the summary below and six publications — printed, accepted, or under review — in international peer-reviewed journals. These publications are referred to in bold face Roman numbers and are included after the summary. Many results from other papers [17–21], as well as unpublished results, are also included in this thesis.

The structure of this summary is as follows. In this section, all of the publications, as well as the author's contribution to these, are presented. A short introduction, presenting the necessary basic concepts and the background of clusters and thin films, is given in section 3. In section 4 an overview of the methods used to obtain the results is given. In section 5, the findings related to epitaxial deposition of clusters are summarized. Film growth by cluster deposition is presented in section 6, and in section 7 the modification of these films is discussed. Finally, the conclusions are presented in section 8.

2.1 Summaries of the original publications

In publication **I**, the effect of surface roughening on the epitaxial alignment of Cu clusters during deposition on Cu (100) substrates was investigated. The research on epitaxial alignment was continued in publication **II**, where the upper limit in cluster size for epitaxial deposition was determined as a

function of both temperature and the amount of clusters that was deposited. The effect of an increased deposition energy on the epitaxial alignment of clusters was investigated in publication **III**. In publication **IV**, variations in the properties of cluster-assembled thin films were studied, for deposition with different cluster sizes and variable deposition energies. The modification of these films by heavy ion irradiation was performed in publication **V**. Publication **VI** regarded the modeling of cluster-surface interactions, based on the experimental observation of spontaneously assembled ring-like structures of supported metal clusters.

Molecular dynamics simulations were the basis for publications **I** – **V**, whereas both experiments and molecular dynamics simulations were used in publication **VI**. Unpublished experimental results are included in Section 7.

Publication I: Inherent surface roughening as a limiting factor in epitaxial cluster deposition, K. Meinander, K. Nordlund, and J. Keinonen, *Nuclear Instruments and Methods in Physics Research B* **228**, 69-74 (2005).

> The effect of surface roughening, caused by hillocks remaining after previously deposited clusters, on the epitaxial alignment of Cu clusters impacting on Cu surfaces was studied with molecular dynamics simulations. It was found that the likelihood of epitaxial alignment for the deposited structures decreases, as the amount of deposited clusters is increased. The result was shown to be dependent on the point of impact of a cluster, relative to the previously deposited clusters.

Publication II: Contact epitaxy in multiple cluster deposition, K. Meinander, T. T. Järvi, and K. Nordlund, *Applied Physics Letters* **89**, 253109 (2006).

> In this study the upper limit in cluster size, for epitaxial deposition of clusters, was determined as a function of both temperature and the amount of deposited clusters. It was shown that the size of clusters that will align epitaxially increases linearly with deposition temperature, but decrease as the amount of clusters is increased. This decrease in cluster size, needed for epitaxial alignment, as the amount of clusters increases, gradually subsides, and approaches a certain lower limit, where epitaxial deposition is possible, independent of the amount of deposited clusters. With cluster sizes below this limit, cluster-assembled thin films will grow epitaxially, whereas with sizes above this limit, thin films will be nanocrystalline.

Publication III: Size dependent epitaxial cluster deposition: The effect of deposition energy, K. Meinander, K. Nordlund, and J. Keinonen, *Nuclear Instruments and Methods in Physics Research B* **242**, 161-163 (2006).

The effect of deposition energy on the epitaxial alignment of nanoclusters during deposition was studied with classical molecular dynamics. The minimum energy needed, in order for Cu clusters of various sizes to arrange epitaxially on a smooth copper substrate at 300 K, was determined. It was found that the time, during which cluster impact zones are at elevated temperatures and pressures, increases logarithmically as a function of cluster size.

Publication IV: Modeling of film growth by cluster deposition: The effect of size and energy, K. Meinander and K. Nordlund, *Physical Review B* **79**, 235435 (2009).

Using molecular dynamics simulations, the variations in density of thin films, grown by deposition of clusters, using various cluster sizes and at different energies, were quantitatively studied. A model explaining the behaviour of clusters, with sizes up to a certain threshold, was presented, and the limit, after which deviations from this model occurred, was determined. A decrease in thin films densities, with increasing cluster sizes, was shown to be caused by a lessened sintering of larger clusters.

Publication V: Irradiation-induced densification of cluster-assembled thin films, K. Meinander and K. Nordlund, *Physical Review B* **79**, 045411 (2009).

The modification of Cu cluster-assembled thin films, using heavy ion irradiation, was studied with molecular dynamics simulations. Irradiation of films, with Xe and Au ions, was carried out with the aim of increasing their densities, without causing a substantial increase in the size of individual nanocrystals. It was shown that densities approaching those of bulk copper can be achieved at heavy ion fluences as low as 5×10^{13} ions/cm^2. Densification was caused by a local melting of individual clusters, and the resulting viscous flow of atoms into voids within the films. Nanocrystallinity was preserved, as recrystallization occurred according to the pre-existing crystal orientations of the clusters.

Publication VI: Self-assembly of supported metal clusters into ring-like structures, K. Meinander, K. Nordlund, and J. Keinonen, submitted for publication in *Nature Nanotechnology* (2009).

The spontaneous formation of μm-sized rings of silica-supported metal clusters was experimentally observed. Using molecular dynamics simulations it was shown that this self-assembly occurs due to the competition between isotropic van der Waals interactions and repulsive dipolar forces, which were induced by the polar substrate. It was shown that, by varying the ratio in strength between the dipolar forces and the van der Waals forces, the shape and size of the ring-like structures could be controlled.

2.2 Author's contribution

The author set up and carried out all of the simulations and analysis of the results in publications **I** – **VI**. In addition the author performed all of the experimental work and analysis in publication **VI**. The author wrote all of the publications in their entirety. The author also implemented and tested the simulation software used in publication **VI**.

3 NANOCLUSTERS

Nanoclusters are agglomerates of atoms or molecules, with sizes in the range of a few nanometers up to several hundreds of nanometers. Nanoclusters differ from *nanoparticles*, in that they are composed of several similar subunits, such as atoms of the same element in, e.g., Cu_N (where N refers to the number of subunits), or small molecules of the same species, e.g. $(SF_6)_N$. Nanoparticles are of the same range in size as nanocluster, but their composition is not as precisely defined.

This section begins with a short description of nanocluster properties, with an emphasis on why these differ from the properties of single atoms or bulk materials. This is followed by a review on cluster-surface interactions, connected to the properties and growth of cluster-assembled thin films.

3.1 Nanocluster properties

The properties of nanoclusters can differ wildly from those of bulk materials [22–24]. This is due to an exponential increase in the surface to volume ratio of the material, leading to an increased percentage of surface atoms, as the size of particles decreases [25]. The role of surface energy becomes more dominant in these spatially restricted systems, which can lead to, e.g., an increased hardness. Strained cluster configurations [26], bound by their high surface energy, have also shown exotic properties, such as a negative heat capacity [27], lowered melting temperatures [28] or the instantaneous transition between solid and molten phases [29, 30]. The structural arrangement of atoms in clusters also follows specific rules, resulting in the existence of *magical numbers* [31] in the amounts of atoms clusters can contain. Clusters that have enough atoms for a specific geometrical shape, or a specific low-energy electronic configuration, are more abundant than others [32].

Clusters also differ in their properties from single atoms, as the confinement of electrons, to the nanoscale size of clusters, adds a new dimension. Through the interplay of delocalized valence electrons in the entire clusters, clusters can behave as a sort of artificial atoms, with electronic energy levels,

resembling those in single atoms, that are size dependent [33]. If the size of, e.g., gold clusters is varied, they go through remarkable changes in both color (from dark red to bright yellow) and chemical reactivity. Small gold clusters will function as catalyst in many reactions, whereas bulk gold is known for its non-reactive properties. Variations in these properties can be fine-tuned, simply by adding or removing atoms from the clusters. Clusters are truly in a size range where every single atom counts, as the addition or subtraction of a single atom brings forth new, unpredictable, properties.

3.2 Cluster-surface interactions

Free nanoclusters are seldom used in applications, as they interact with their surroundings very reactively. Cluster usually appear as immersed in solutions, bound in a matrix, or as deposited on surfaces. The clusters studied in this thesis are mainly deposited on surfaces by some physical deposition scheme. When depositing clusters on surfaces, it is vital that the interactions between a cluster and the specific surface are known.

If clusters are deposited at low energies, the interaction between the cluster and the surface itself is of utmost importance in deciding the outcome of the deposition event. Depending on the binding energy between the cluster and the substrate, as well as phenomena induced by physical or chemical properties of the surface, many different things can occur. If there is a strong attractive interaction between the cluster and the surface, a large *wetting* of the surface will occur, i.e., the cluster will spread out, and eventually form an island, with a thickness of a few atomic layers, on the surface. If the crystalline lattice of the cluster matches that of the substrate, there also exists a possibility that the cluster will adopt an epitaxial alignment [34], i.e., orient itself in the same crystalline direction as the substrate.

If the interaction between the cluster and the surface is weak, at least in the case of low-energy deposition, the contact area between the cluster and the surface will be smaller, and clusters will usually have a large mobility on the surface. This allows for a fast diffusion of clusters, and a higher degree of cluster-cluster interaction, usually resulting in the growth of exotic structures. Clusters with high mobility, will normally stick to each other, and cover the surface with branch-like structures [35], unless the clusters are guided by other forces (as was the case in publication **VI**).

When deposited at higher energies, the energy density at impact will cause a melting of the cluster and its nearest surroundings [36]. The collective collision effect of a multiple atom projectile will be a large lateral spreading during impact [37, 38], which automatically induces a smoothing of the local neighbourhood at the impact zone [39, 40]. When deposited at high energies, clusters can be used, e.g., for the machining of selected surfaces, or as a means of growth for films with high adhesion.

Deposition at higher energies may also result in the formation of local defects in the structure of the surface. Deposited clusters will usually stick to these defect sites, and a high mobility and surface diffusion of clusters, deposited at high energies, is therefore very unlikely. This is the case even if the interaction between the clusters and the surface is weak in its nature.

3.3 Cluster-assembled thin films

The prospect of using nanocluster deposition for the growth of thin films has been widely researched during the past few decades [35]. When clusters are deposited at high energies, independent of surrounding conditions, they will form a smooth, hetero- or homoepitaxial film, which has good adhesion to the substrate [41–44]. On the other hand, if low energy is used, there is a possibility of transferring some of the inherent properties of the nano-scale structure of the clusters to the film itself [45]. This opens up a world of possibilities for the use of clusters in thin film growth.

Nanocrystalline films are films which contain many nanometer-sized regions with different crystal orientations. Due to an increased amount of grain boundaries within these films, which prevents the migration of defects and dislocations that make a material weaker, many nanocrystalline materials can be much harder than their normal counterparts [46]. Film growth, through the deposition of nanoclusters, is a very promising method for the production of nanocrystalline films. A transfer of the enhanced electronic and optical properties of clusters, such as a high photoluminescence [47, 48], to thin films, is also highly lucrative application for the use of clusters in thin film assembly.

3.3.1 Thin film growth

Film growth, by deposition of clusters, differs from growth with single atoms in that every single impact accompanies a higher energy density in the impact zone [36]. This will lead to a behaviour that is very much different from any single atom deposition methods. Multiple near-surface collisions hinder penetration, and any melting or atomic rearrangement during the cluster impact will therefore be a shallow event [42, 49–51]. High growth rates can also be achieved, as the amount of atoms impacting in a small area is much larger than what can be achieved by any single atom deposition methods. Cluster deposition extends the achievable conditions of deposition to a parameter region, in both deposition energy and atomic fluence, that is currently very poorly charted [52].

Both cluster-surface and cluster-cluster interactions must be understood well, before a reasonable understanding of the growth mechanisms and the final properties of cluster-assembled thin films can be achieved. The results of this thesis bring us one step closer to this final goal.

4 METHODS

The combination of experiments and computer simulations adds diversity to traditional scientific research. Experimental methods, if performed correctly, will always give correct results, but due to the lack of sufficient *in situ* analysis methods, which would possess both good resolution and a rapid measuring speed, physical mechanisms are not always deducible from these. Computer simulations, on the other hand, can offer an atomic (or even electronic) resolution and will elucidate mechanisms on the atomic time-scale. These, however, rely heavily on approximations, and only with difficulty can they span over several magnitudes of time.

Through the combination of both methods, one can often compensate for the deficiencies that either method, when used separately, presents. Experiments will provide an easily ascertainable end-result from a well known initial configuration, and computer simulations, knowing both initial and final configurations, can provide a plausible explanation to what physical mechanisms could have contributed during the experimentally observed phenomena. If performed in the opposite order, computer simulations can predict end-results, through the simulation of well-known mechanisms, which can then later be experimentally confirmed. Computer simulations, such as molecular dynamics simulations can, in a sense, be used to either predict or confirm hypotheses based on experimental results.

The combination of both molecular dynamics simulations and experimental methods has been successfully implemented in this thesis. In publication **V**, the densification of cluster-assembled thin films was predicted with simulations, and was only later successfully confirmed in the experiments presented in Section 7. The ring-like assembly of silica-supported metal clusters, in publication **VI**, was initially an experimental observation, the mechanism of which could only later be explained with the use of molecular dynamics simulations.

Classical molecular dynamics has been the main method used in publications **I** – **V** of this thesis, whereas a combination of experiments and molecular dynamics simulations were used successfully in publication **VI**. Several experimental results, yet to be submitted for publication, are presented in Section 7.

4.1 Molecular dynamics

Classical molecular dynamics (MD) is a method where the Newtonian equations of motion are numerically solved for a given system of particles, the interaction of which is governed by a model describing the forces between these particles [53]. MD was originally developed in the late 1950s,

and used for the study of atomic vibrations in molecules [54, 55]. An advantage of molecular dynamics simulations over experiments is that systems can be studied with an atomic resolution at short time- and length-scales, down to femtoseconds and ångströms. These small scales are, however, also the major limitation of MD – events lasting for microseconds or longer, or systems of large sizes, cannot easily be studied.

Using a classical model to describe the force, the equations of motion are solved for each atom in the system, and integrated over a small time-step. The time-step is kept small enough to allow for a conservation of the total energy of the system. Often a variable time-step can be used, in order to speed up the calculations [56]. Several approaches have also been taken to improve the outcome of these calculations. Predictor-corrector algorithms are, for instance, generally used, where the movement of atoms over one time-step in the simulations is slightly corrected, once the forces between atoms in their new positions are known.

Interaction models used in MD are usually very simplified from the more fundamental models. This is done in order to speed up calculations, but, if assumptions are too severe, it can also result in incorrect results. E.g., the Born-Oppenhiemer approximation [53], which is based on the assumption that electrons move fast enough to reach equilibrium much faster than the atomic nuclei, is routinely used in classical MD. According to this, the dynamics of the electrons can be separated from that of the atomic nuclei, making it possible to de-couple any electronic contributions from the atomic interactions. The interaction between electronic vibrations and vibrations of the atomic lattice, through the so-called electron-phonon coupling, can, however, have a considerable effect on, i.e., the cooling of atomic systems [57, 58]. It is important to realize that the force model limits the properties of a system that can be investigated; any model that, for instance, excludes the electronic degrees of freedom will fail when investigating phenomena that are sensitive to the interactions between electrons.

The MD simulations from publications **I** – **V** were performed with the simulation code PARCAS written by Kai Nordlund [56, 59, 60]. Within this code, the fifth-order Gear predictor-corrector algorithm (Gear5) [55] is utilized to solve the equations of motion. A variable time-step was used in the simulations, to ensure a short enough change in time when energetic particles were present. A separate MD code was developed by the author, for the simulations performed in publication **VI**.

4.1.1 Interatomic potentials

In classical MD simulations, the forces between particles in the system are derived from a potential energy function, whose functional form is often based on a quantum mechanical treatment of the system. The more fundamental quantum mechanical treatment is simplified, by the use of various

parameters, the values of which are taken either from first principle calculations or from fits of the model to experimental data. If the latter is used, the potential model is called semi-empirical.

The potential energy of an atom depends on its surrounding atoms. If the energy can be calculated by summing up terms, which depend on the atom under consideration and only one of any of its surrounding atoms, this potential is called a pair potential. If the energy, on the other hand, depends on the environment in a more complicated manner, so called many-body potentials must be used.

Semi-empirical potentials, based on the Embedded Atom Method (EAM) by Daw, Baskes, and Foiles [61–63], were used to model the interactions between metal atoms in the simulations of this thesis. Pair potentials were used to model the interaction between rare gas atoms and metal atoms.

EAM potentials are many-body potentials, mainly suited for the modeling of metal-metal interactions. According to the model, a metal atom can be considered to consist of a positive "ionic core" (the atoms with their valence electrons removed), embedded in a "sea" of electrons. If the energy needed to add an atom, or ionic core, to this system of electrons, the *embedding energy*, is G, then an expression for the total energy of the system can be written as

$$E = \sum_i G_i \left[\sum_{j \neq i} \rho_i^a(r_{ij}) \right] + \frac{1}{2} \sum_{i,j(j \neq i)} v_{ij}(r_{ij}), \tag{1}$$

where $\rho_i^a(r_{ij})$ is the electron density of the atom j, which is at a distance of r_{ij} from the atom i, and v_{ij} describes the two-particle interaction between these atoms. The EAM potential is a many-body potential, as the effect of many atoms, not just two, is included in the embedding function.

At small interatomic distances, all of the potentials, describing both metal-metal interactions and interactions between rare gas atoms and metals, were smoothly joined to the universal repulsive Ziegler-Biersack-Littmark (ZBL) potential [64], to realistically describe high-energy collisions and the interaction of atoms at these small distances. The interaction between metal atoms of different species can easily be modelled in metal alloys, by combining the EAM potentials of single elements, into EAM cross-potentials [63, 65, 66].

Potentials are often cut off at some interatomic separation, the *cut-off* distance, in order to reduce the amount of computational time needed. If the potentials are not cut off, all of the atoms in the system would have to be included when calculating the force on any particular atom, which would make the simulations extremely slow. The cut-off is usually a "smooth" cut-off, meaning that the potential gradually approaches zero as the cut-off distance is approached.

4.1.2 Modeling of cluster deposition

When modeling the deposition of clusters on surfaces, a free surface on a larger bulk substrate is needed. This is achieved by using *periodic boundary conditions*, i.e. a condition in which an atom at the end of the simulation cell (the simulated volume) will interact with atoms at the opposite end, in two of the three Cartesian directions, x, y, and z. If an atom passes over this periodic boundary it is made to reappear at the other end of the simulation cell.

If a free surface in the z-direction is desired, a rectangular cell, with periodic boundaries in the x- and y-directions is required. In order to mimic a larger surrounding bulk region, temperature scaling is also employed in these directions, near the borders of the cell. Temperature scaling, in the simulations of this thesis, was implemented using Berendsen's temperature control algorithm [67], which forces the temperature (i.e. the velocities of the atoms) in the scaled region to approach some predefined value at a certain rate. The bottom of the cell, one of the "free" surfaces in the z direction, must also be fixed, i.e., the velocities of the atoms are kept at zero, and temperature scaling must be applied to a few layers above this, in order to realistically mimic a thicker substrate. Any heat or pressure wave incident on the temperature-scaled regions will be damped, similarly to what would happen if the bulk substrate truly was larger.

When depositing on copper, the substrate was prepared so that the free surface would be a (100) surface, and the copper clusters were given the shape of Wulff polyhedra [68] with the dimensions of each cluster volume optimized to the configuration with minimum surface energy. This shape has been found to be one of the common shapes for small Cu nanoclusters [69–71]. Simulations with spherical clusters cut out from a perfect face-centered cubic (FCC) lattice, and with multiply twinned icosahedra, which are considered to be the lowest energy structures for copper clusters containing less than ~ 200 atoms [72], were also performed. There were no significant differences in the results for these, indicating that the behaviour during deposition is not sensitive to the exact initial shape of the cluster (at least as long as the atom structure is close-packed) [17].

Prior to deposition, the atoms of each cluster and substrate were given initial random velocities, corresponding to the temperatures that were desired, and each system was separately relaxed, for approximately 20 ps, using the temperature control scheme. The actual deposition was then performed by rotating the cluster with a random angle, placing it above the substrate and then giving it a velocity in the direction of the substrate, with a kinetic energy corresponding to the desired deposition energy. After deposition, all systems were relaxed for 1.5 – 2.0 ns.

4.1.3 Thin film growth and ion bombardment

The simulation process for film growth was as follows. The clusters and substrate were created separately and allowed to relax before being combined. Substrate sizes were chosen such that their lateral dimensions were three times larger than the diameter of the clusters that were to be deposited. Deposition, for each individual cluster, was performed in the same manner as during single cluster deposition. After impact of the cluster on the surface of the substrate, the film structure was allowed to relax for 100 ps before the following cluster was deposited. Between each impact the substrate and any previously deposited cluster-structure was translated randomly through the periodic boundaries of the simulation cell, in order to allow for random impact points. Each cluster was rotated to a random orientation before being deposited at the center of the newly translated substrate. This process was repeated until 50 clusters had been deposited.

Irradiation of the cluster-assembled thin films, with the purpose of increasing their density, was performed in a similar manner. The substrate was translated by a random distance through its periodic boundaries before each ion impact, whereupon an ion of the correct species was created above the center of the substrate and given a velocity corresponding to the correct kinetic energy in a direction directly towards the substrate. Irradiation was performed in this manner to insure that impacts would occur in random positions, but sufficiently far away from the borders of the simulation cell. After each impact, the cell was relaxed for 100 ps, after which the temperature was quenched down to the initial temperature (300 K) over the final 2 ps. The decrease in temperature during quenching was seldom more than a few tens of degrees, as most cooling had already occurred during the initial relaxation. Inelastic energy losses, due to electronic stopping, were included in the calculations for all atoms with kinetic energy higher than 5 eV [64].

4.2 Experimental cluster deposition

The first instruments built explicitly for use as nanocluster sources, relied on a fast evaporation of the cluster material into an inert gas [8–11]. Clusters were allowed to condensate at high vapour pressures in the quasi-equilibrium conditions of the chambers. Modern day sources, of, so-called, condensation-cell type, rely on similar methods [24, 73].

In Fig. 1(a) a schematic diagram of a condensation-cell-type cluster source is shown. The basic operating principle of sources of this type is as follows. Cluster material is sputtered, by a large magnetic field, from the target situated on the magnetron, a flow of inert gas then sweeps the vaporized atoms further into the condensation chamber, where the vapour cools down through collisions with

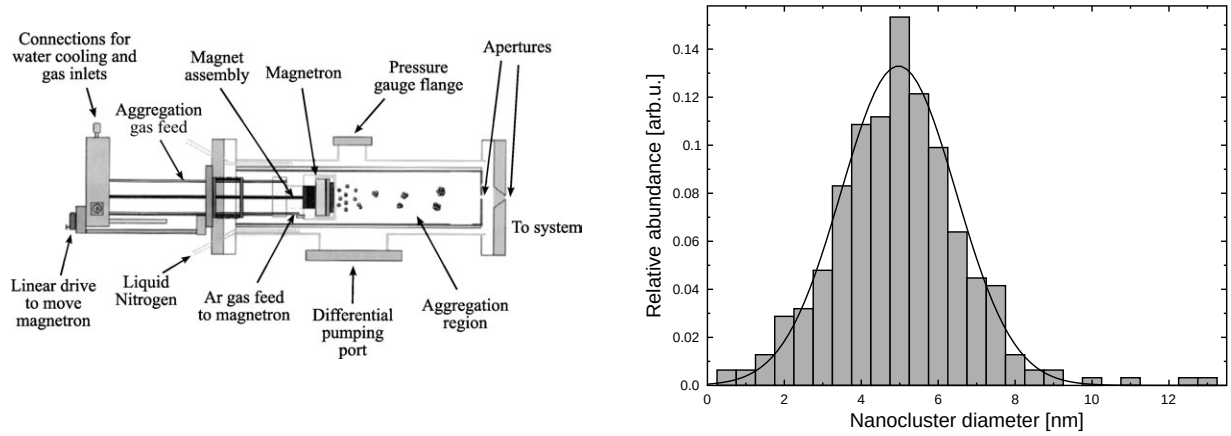

(a) (b)

Figure 1: (a) A schematic diagram of a condensation-cell-type cluster aggregation source. Clusters of any metal or semiconductor material, as well as many ceramics, can be produced with a similar source. (b) The size distribution of Cu clusters produced at maximum aggregation length, with cooling at 300 K, and Ar flows to the magnetron and aggregation chamber, $Q_m = 50$ cm^3/min and $Q_a = 150$ cm^3/min, respectively. The solid line is a Gaussian fit to the experimental data.

the inert gas. From the super-saturated vapour, clusters then condensate, after which they are swept out of the chamber by the inert gas flow. Differential pumping at several stages is necessary, in order to minimize the load of aggregation gas entering the deposition chamber.

The size of the produced clusters depends on the magnetron power, i.e., the speed at which cluster material is vaporized, the length of the aggregation region, the pressure and temperature within the condensation chamber, and the speed at which the inert gas flow sweeps vaporized material from the magnetron. A typical size distribution of clusters, produced with a condensation cell-type source is shown in Fig. 1(b). After extraction of the clusters from the condensation cell, further manipulation can occur. The first stage of this manipulation is typically an ionisation of the clusters, after which they can be more easily handled trough the use of ion-optics. The use of electrical fields for size-selection and acceleration of cluster beams is typical in cluster deposition applications.

The University of Helsinki Facility for Nanocluster Deposition (FaNaDe), consists of a condensation-cell-type source connected to an ultra-high vacuum (UHV) chamber, which in turn is connected to a UHV transfer line, with which samples can be moved to other chambers, mostly for the purpose of analysis, whilst still remaining in ultra-high vacuum conditions. UHV is a prerequisite for the study of nano-scale structures on surfaces, as oxidation is a rapid event in atmospheric conditions. A voltage (0 – 30 kV) can be applied to the entire cluster source, allowing for the acceleration of ionized clusters

towards a neutrally charged sample. Size analysis of the produced cluster beams is performed with a quadrupole mass filter.

4.3 Atomic force microscopy

Scanning probe microscopy (SPM), founded by the invention of the scanning tunneling microscope (STM) by Binning and Rohrer [2] in 1981, is extremely suitable for the analysis of nano-scale structures on surfaces [74–77]. In SPM, images of the sample surface are obtained by mechanically moving a physical probe in a raster pattern over the specimen, line by line, and recording the probe-surface interaction as a function of position. Different types of interactions are used, depending on the specific SPM method. In scanning tunneling microscopy, for instance, the current of electrons tunneling between a conductive surface and a sharp metal tip is measured, a phenomenon which is exponentially dependent on the interaction distance [78].

In atomic force microscopy (AFM), the sample surface is probed with a sharp tip, a couple of μm:s long and often less than 100 Å in diameter, located at the free end of a cantilever that is 100 – 200 μm long [78]. Forces between the tip and the sample surface, van der Waals forces, among others, cause the cantilever to bend, or deflect. Van der Waals forces exist between all types of materials, making AFM a suitable technique for any surfaces. Bending of the cantilever can be measured by bouncing a laser beam off the cantilever end onto a position-sensitive photodetector (PSPD). This bending is countered by moving the sample either closer or further away from the AFM tip, using feedback electronics. A topographical image of the sample surface can then be extracted directly from the feedback signal. A schematic diagram of an AFM measurement system is shown in Fig. 2(a), and in Fig. 2(b) the relationship between distance and force for the van der Waals interaction is displayed.

The resolution of an AFM is dependent on the ability of the piezoelectric elements of the scanner to execute motions, with a precision and accuracy at the atomic level or better, on electronic commands. Typical height resolution during AFM measurements is in the range of 0.1 Å. In the lateral directions, resolution is however also limited by the physical properties of the AFM tip. Two factors of the tip shape affect the outcome of images: the end radius of the tip, and its aspect ratio, i.e., the ratio between the length and the width of the tip. The end radius of the tip defines the minimum distance at which features on a surface must be separated, in order for them to be imaged as individual objects. The aspect ratio, on the other hand, affects the angle at which the sides of the tip protrudes. If this angle is too large, interaction between the surface and the sides of the tip may occur.

As long as an AFM tip is sharper than any surface feature being imaged, the true edge profile of the feature will be represented. If, however, sharper features are present on the surface, the image will be

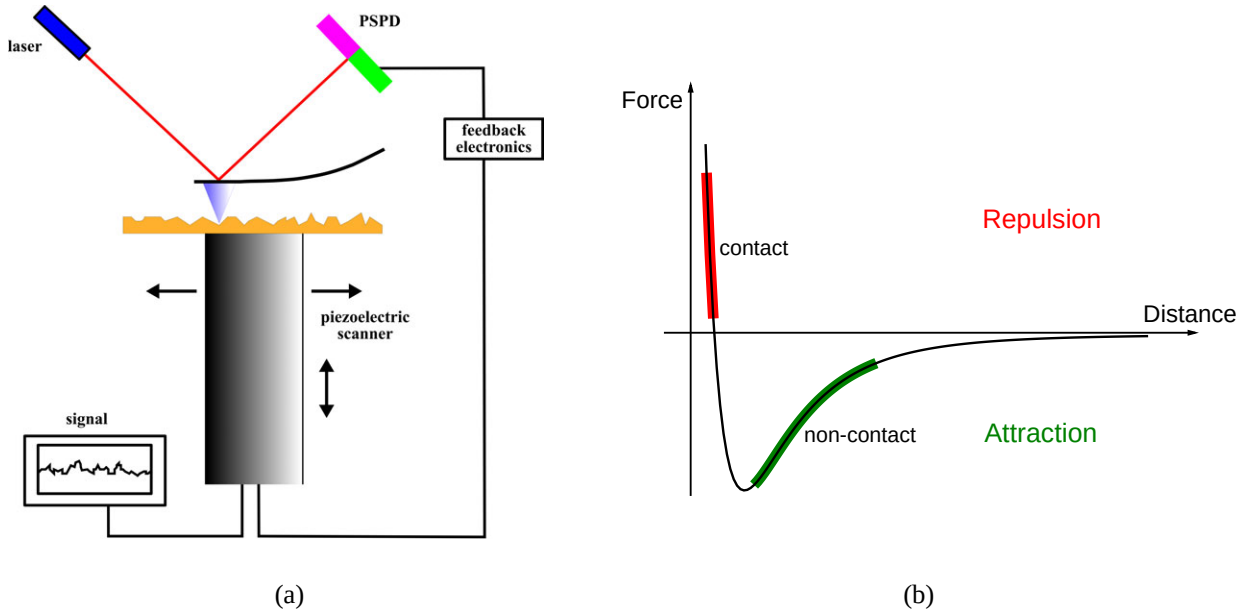

(a) (b)

Figure 2: (a) A schematic diagram of an atomic force microscope (AFM). Images are created through movement of the piezoelectric scanner, giving a resolution of ~ 0.1 Å. Movement of the AFM cantilever is detected by bouncing a laser beam off the end of the cantilever onto a position-sensitive photodetector (PSPD), upon which the sample is either lowered or raised to compensate and cancel this movement. The AFM topographic image is directly acquired from the signal of this feedback process. (b) Van der Waals forces govern movement of the AFM cantilever, resulting in either an attractive or repulsive interaction, depending on the distance between the tip and the sample surface. Different modes of measurement utilize different regions of the force curve.

dominated by the shape of the tip. This is known as *tip convolution*, when the edge of the tip, rather than the end of the tip is interacting with the feature, and every point in the image represents a spatial convolution of the shape of the tip and the shape of the feature imaged. Because of this, the lateral dimensions of features in AFM images are quite often highly exaggerated [78].

Commercial AFM tips are commonly pyramidal or cone shaped with a sidewall angle of 20° – 40° and an end radius of 10 – 35 nm. Because many samples have features with steeper sides than this, tip convolution is a common occurrence in images. Although tips with an end radius of below 1 nm have been developed, it is more difficult to produce AFM tips with a high aspect ratio. Angles of $\sim 10^\circ$ have been obtained, but for tips sharper than this, the result is often a degraded durability or even a bending of the tip during measurements.

4.3.1 Measurement modes

Depending on the properties of the surfaces being imaged – roughness, hardness, elasticity, etc. – different *modes* of AFM imaging can be conducted. In *contact* mode AFM, the AFM tip makes soft

"physical contact" with the sample, working in the repulsive region of the van der Waals force curve. Contact mode offers the best resolution of all the AFM modes in ambient conditions. Contact mode AFM can operate in either *constant-height* or *constant-force* mode. In constant-height mode, the spatial variation of the cantilever deflection is used directly to generate the topographical data, as the height of the scanner is fixed as it scans. This provides high resolution images, but is limited to smaller surface areas, with very minimal variations in height. Constant-force mode, the more commonly used measurement mode, allows for a higher flexibility, as the force between the tip and the surface is kept constant by an up-down movement of the scanner, guided by the feedback circuit. The image is generated from the scanner's motion, which allows for larger areas and greater variations in height.

Non-contact AFM differs from contact mode AFM, in both the region of the van der Waals curve at which it operates and the means to detect tip-surface interactions. Non-contact AFM is one of several vibrating cantilever techniques, in which an AFM cantilever is vibrated at a high frequency near the surface of the sample. Because forces between the tip and the sample are very low in the non-contact regime, a very sensitive detection scheme must be used. Stiff cantilevers are usually used in non-contact AFM, where the system vibrates the cantilevers near their resonant frequencies (typically from 50 to 400 kHz), with an amplitude of a few tens to hundreds of ångströms. The system then detects changes in the resonant frequency or the vibrational amplitude, as the tip comes closer to the sample surface, where it is affected by attractive van der Waals forces.

The benefit of using non-contact measurements, is a lower degree of degradation of the AFM tip and of the sample surface. Lateral forces between the tip and the surface, which may result in the unintentional displacement or destruction of surface features, are also completely eliminated. In UHV conditions, non-contact imaging may sometimes offer the best resolution achievable with AFM techniques, although at ambient conditions the result is always poorer than with contact mode imaging. Often samples will be covered by a thin layer of liquid water, if they are measured in the open atmosphere. In non-contact mode, the surface of this liquid layer will be imaged, rather than the topography of the underlying substrate.

A third mode of AFM operation is also available, *intermittent-contact*, which combines the benefits of both contact and non-contact AFM. Intermittent-contact, or *tapping mode* AFM, is similar to non-contact AFM, except that the vibrating cantilever is brought closer to the sample surface, so that it just barely hits, or "taps", the sample when it is at its lowest point. In tapping mode the cantilever's oscillation amplitude changes in response to the tip-sample distance, and the surface topography can be imaged by monitoring the movement of the scanner as it counters these changes. Intermittent-contact AFM eliminates the lateral forces of contact mode AFM, and is therefore less likely to cause damage to the tip or the surface, but it still offers a tip-surface interaction strong enough to penetrate

the liquid layer present on most samples. All AFM measurements performed in this thesis have been conducted in the intermittent-contact mode of operation.

5 CLUSTER DEPOSITION

The interaction between clusters and surfaces is of vital importance during the physical deposition of clusters. Depending on the type of surface and the physical properties of the clusters, severe variations in the resulting structures can be observed. Small changes in factors such as cluster size, deposition energy, and cluster or substrate materials will result in final structures that can range from perfect epitaxial films to an exotic self-assembled arrangement [79–82]. This section concerns the effects of cluster-surface interactions studied in publications **I** – **III**, and **VI**, as well as Ref. [17] and [19].

5.1 Epitaxial alignment

If clusters are deposited, with low energies, on the clean, single-crystal surfaces of materials with crystallographic lattice spacings equal or close to the material of the cluster, an epitaxial alignment of the cluster can occur [34, 83–85]. If a cluster is completely epitaxially aligned, all of its atoms have adopted the same crystalline orientation as the atoms of the underlying substrate. This alignment is facilitated by a strong interaction between the cluster and the surface, especially for cases of similar materials, where wetting is substantial.

Snapshots of a typical deposition event can be seen in Figure 3, were the low-energy impact (deposition energy is 5 meV/atom) of a Cu_{826} cluster on a smooth Cu (100) surface is shown from a side-view. As the cluster approaches the surface, it accelerates rapidly and impacts with a kinetic energy considerably higher than the given deposition energy. This acceleration is caused by the release of a binding energy between the cluster and the substrate [34], which is supplied by a lowering of the total surface energy of the system. This release of binding energy is responsible for most of the rearrangement of the cluster atoms during the first few picoseconds after the impact.

If enough energy has been released during impact, a complete epitaxial alignment can occur. This is not the case for the cluster in Fig. 3, where a large grain (a region which has adopted a crystallographic orientation that is different from its surroundings) is present in the upper part of the cluster. This offers a good example of a non-epitaxially deposited cluster.

The epitaxial alignment of a cluster deposited with a low deposition energy, on a smooth surface, will depend on two factors. These are, the size of the cluster, and the temperature at which it is

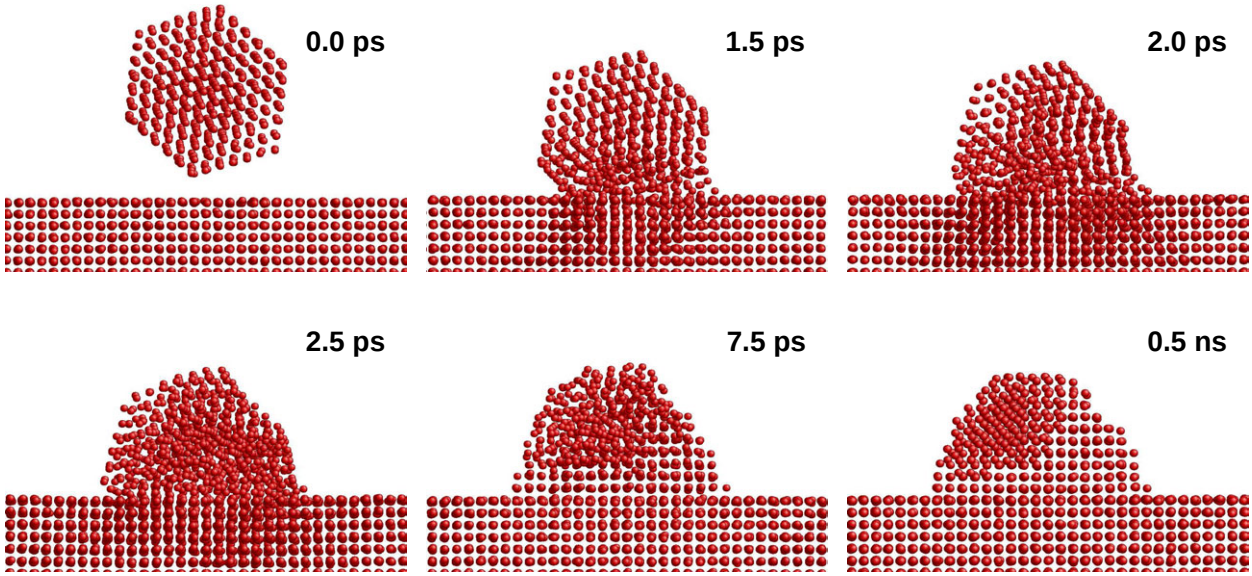

Figure 3: Snapshots, showing the side view of a typical low-energy deposition event (5 meV/atom), where a Cu_{826} cluster impacts a Cu (100) substrate. After relaxation, a large grain remains in the upper part of the deposited cluster, as the impacting cluster is too big for epitaxial alignment.

being deposited. Alignment itself is achieved through the contribution of two separate mechanisms – the short time-scale event of initial rearrangement of the cluster atoms upon impact, and the longer time-scale event of grain boundary diffusion, caused by the thermal movement of atoms. These were studied in publications **I** and **II**, as well as Ref. [17] and [19].

5.1.1 Initial rearrangement

When single clusters impact on a smooth surface, the release of binding energy can be observed as an increase in the temperature of the cluster atoms and the local surroundings of the impact zone. In Figure 4(a) this is illustrated for the case of a Cu_{25} cluster impacting a Cu (100) substrate at 0 K. At this microscopic scale, temperature is understood as the average kinetic energy of the atoms in the system. This increase in kinetic energy is drawn from a decrease in the total potential energy of the cluster-surface system, as the total surface area is decreased upon impact. The potential energy, stored in surface energy, decreases, when surface areas of both the cluster and the substrate are annihilated.

If epitaxial alignment occurs, as a result of the cluster impact, the potential energy of the cluster atoms will settle at its lowest level, whereas in other cases it will remain at some higher level. This is illustrated if Fig. 4(b), where the average potential energy of the cluster atoms is plotted for deposition with various sizes of clusters on a smooth Cu (100) surface. The final value of the average potential

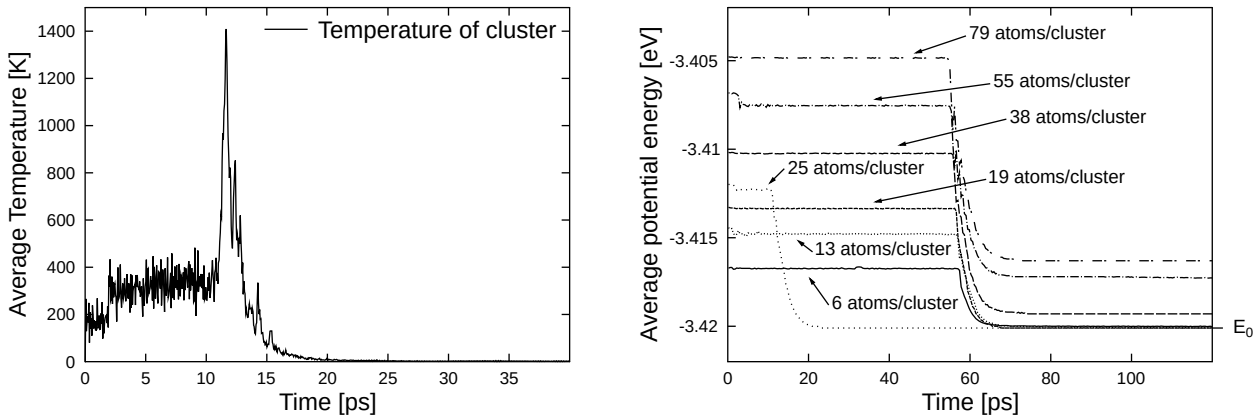

(a) (b)

Figure 4: (a) The temperature increase in a Cu_{25} cluster impacting a Cu (100) surface, at 0 K, as a function of time. A rapid increase in the cluster's temperature occurs, as the cluster hits the surface after approximately 12 ps. (b) Change in the average potential energy for the atoms of a cluster, when Cu clusters of different sizes are impacting a Cu (100) surface, as a function of time for deposition at 0 K. The 6, 13, 19, and 25 atom clusters were within the size limit for epitaxy, whereas the 38, 55, and 79 atom clusters were not. E_0 is the average potential energy of an epitaxial system. From [17].

energy approached the same value for all epitaxial systems in these cases. The average potential energy of clusters that have not achieved epitaxial alignment, on the other hand, has settled at higher levels.

The degree at which the potential energy is lowered is highly dependent on the size of the clusters which are being deposited. In general, the total amount of potential energy released, the binding energy of the cluster to the surface, will increase as the cluster size increases. This is simply because the total annihilated surface area will be larger for larger clusters. The same cannot, however, be said for the decrease in average potential energy, the critical value to be compared with average kinetic energy and temperature, as the ratio between cluster surface and volume will decrease as cluster size is increased.

Epitaxial alignment can occur directly after impact, if the increase in temperature of the cluster atoms is high enough to completely melt the cluster. This occurs if the temperature increases past the mechanical melting point of the cluster material, i.e., the temperature at which melting occurs even without nucleation points [86–90]. When a cluster lands on a surface, the released energy, ΔE, will approximately equal the loss in surface energy

$$\Delta E = 2\gamma A, \tag{2}$$

where γ is the surface energy and $2A$ is the surface area lost in the collision. The energy which goes into heating the cluster will be approximately half of this, as half of the energy will most probably be transferred to the substrate.

The contact area, A, between a cluster and a smooth surface can be calculated by approximating the cluster as a sphere, and estimating A as the area of its segment, with a height h, the interaction range between the atoms of the cluster and the surface. This gives us $A = 2\pi rh$, where r is the radius of the cluster. If h, is set as one lattice constant [19], $h = a$, the total released energy will be $\Delta E = 2\gamma\pi ra$.

The change in temperature needed to achieve the melting point for a cluster, T_{melt} is $\Delta T = T_{\text{melt}} - T_i$, where T_i is the initial temperature of the cluster. If the energy required for this heating is equal to the surface energy released to the cluster, this gives the relation

$$\frac{3}{2}Nk_B\Delta T = \frac{\Delta E}{2}, \tag{3}$$

where N is the number of atoms in the cluster, $N = \frac{16\pi r^3}{3a^3}$. The released energy is divided by two, due to the equipartition theorem. For the limiting cluster size, we therefore have the expression [19]

$$r_{\text{crit}} = \sqrt{\frac{\gamma a^4}{8k_B}}\frac{1}{\sqrt{T_{\text{melt}} - T_i}}. \tag{4}$$

Clusters with sizes below this will, consequently, melt completely, and can be expected to recrystallize according to the already existing crystal lattice of the substrate, thereby aligning completely epitaxially.

Due to the increase in temperature, which occurs directly after impact, there is an initial period of disorder for the cluster, after which it rapidly recrystallizes, either partly or completely epitaxially. If grains remain in the upper portions of the deposited cluster, rearrangement can, however, still occur, if temperatures are high enough.

5.1.2 Grain boundary movement

Even after the initial rearrangement of the cluster atoms, during the period immediately after impact, has ceased, thermally activated mechanisms can further the evolution of the clusters towards an epitaxial alignment [17, 19]. If small enough grains remain in the upper parts of the cluster, and temperatures are high enough, the thermal movement of atoms can lead to an incorporation, and realignment, of these grains according to the underlying lattice [91, 92].

A vast majority of the grains are connected to the epitaxial part of the cluster by {111} twin boundaries [19, 93, 94]. The energy of these twin boundaries is very low, compared to e.g. the surface energy, and they are therefore mobile at fairly low temperatures. The added strain of the cluster-hillock, will further decrease the potential barrier, lowering the activation energy of this movement. At higher temperatures, the thermally activated motion of these twinning boundaries can be fast enough to push through the entire grain in a fairly short span of time.

If grains are small enough, the energy barrier for grain boundary motion will be sufficiently low for the thermal movement of atoms to cause twinning dislocations (more specifically Schokley partial dislocations [19, 95]), to move throughout the cluster, resulting in a shift of the grain boundary further into the grain. Once this happens, the rest of the non-epitaxial layers will glide the same way, leaving behind a perfect FCC lattice.

If allowed to relax for even longer times at sufficiently high temperatures, epitaxial cluster hillocks will eventually form atomic monolayers, through long-time-scale thermally activated surface migration [96]. The times required for a flattening of this kind, range from milliseconds for smaller grains, up to several hours for larger ones. During actual cluster deposition, time between impacts, given typical fluxes of the order of 10^{12}-10^{15} clusters/(cm^{2}s), will on average approach the order of milliseconds, rather than the 2 ns used in our simulations. Cluster hillocks will experience significant flattening at temperatures around and above 300-500 K, thereby improving conditions for clusters deposited on top of them.

5.1.3 Multiple clusters

If cluster deposition continues beyond deposition of the first monolayer, incoming clusters will eventually impact on the hillock-like protrusions remaining after previously deposited clusters [97]. The surface roughening caused by previously deposited clusters will affect the cluster-surface interaction for these following clusters (publication **I**). This can clearly be seen in Fig. 5, where a schematic

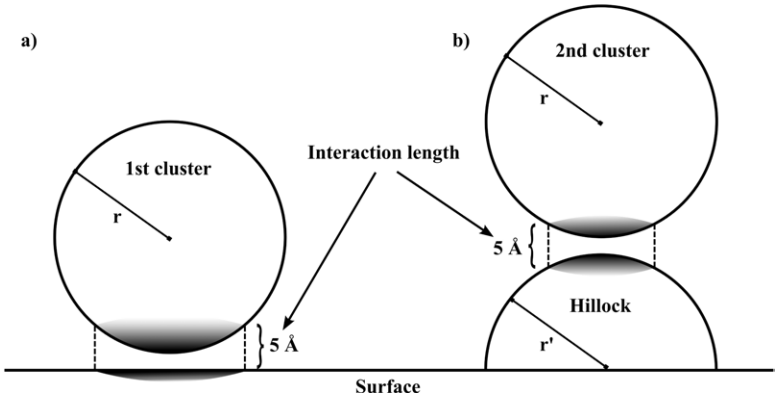

Figure 5: Schematic diagram, showing the difference in projected surface area of interaction between a) a cluster and a smooth surface, and b) a cluster and the hillock remaining after a previous cluster impact. Due to the smaller interaction area of the latter, the temperature increase of the cluster atoms, and therein the likelihood of epitaxial alignment, will be lower.

drawing of the difference between deposition on a smooth surface and deposition on a roughened surface is presented.

The interaction area between an incoming cluster and a smooth surface is very much larger than for the case of a cluster impacting on a previously deposited cluster. This is mainly due to a high local curvature of the surface, roughened by the previously deposited cluster, at the impact point of the second cluster. For equisized clusters, it can geometrically be shown that the total surface area, which is lost in the collision between the second cluster and the hillock remaining after the first, will be approximately half of what was lost in the collision between the first cluster and a smooth surface. This decrease in the interaction area for the second cluster will result in a lower initial release of binding energy at impact, and therefore a lesser increase in the local temperature of the impact zone. In Fig. 6(a) the decrease in potential energy upon impact of the first, second and third Cu_{38} cluster is shown, together with the associated increase in temperature of the cluster atoms in Fig. 6(b).

As the increase in the temperature of the cluster atoms, during the impact of the second cluster, is much lower than for the corresponding case of deposition on a smooth surface, the initial amount of rearrangement of the cluster atoms will not be as extensive. This decrease in initial rearrangement will eventually lead to a lesser likelihood of an epitaxial alignment of the deposited cluster structure. In Fig. 7, the maximum size of the clusters that can be deposited, in order for the final structure to achieve complete epitaxial alignment, for the case of multiple amounts of clusters deposited on top of each other, is shown. As can be seen, the upper limit in cluster size decreases for every new cluster

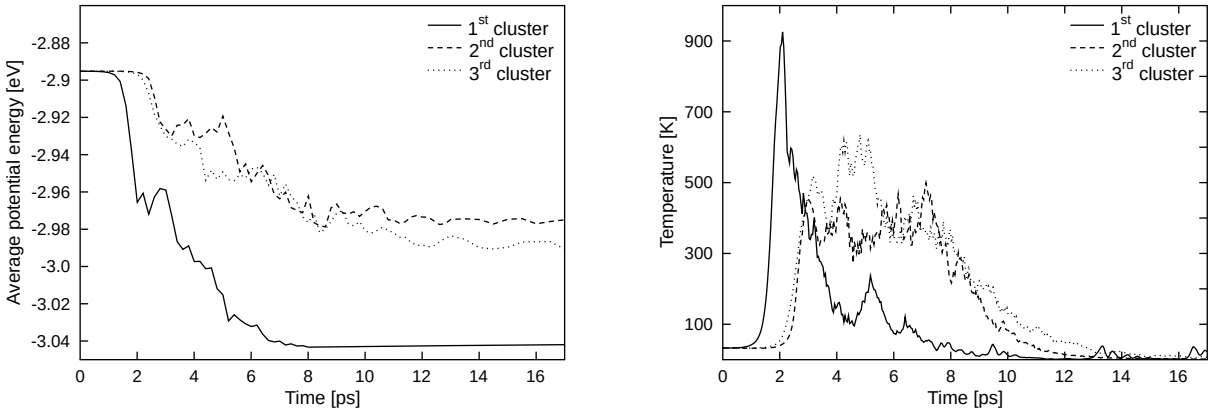

(a) (b)

Figure 6: (a) The average potential energy of the atoms in the first, second and third Cu_{38} cluster deposited on a smooth substrate at 0 K, as a function of time after impact. (b) The local increase in temperature associated with each cluster impact. The decrease in potential energy, i.e. the binding energy released during impact, is much lower for the second cluster, as compared to the first. This is due to the curvature of the surface roughened by the hillock remaining after the first impact. The potential energy curve for the third cluster is very similar to that of the second, as the curvature of the surface remains roughly the same, independent of the amount of deposited clusters. From publication **II**

that is added. Long time-scale effects still exist, but the decisive factor in this lowering of the limit is the initial release of binding energy that will heat up the cluster atoms.

The upper limit in cluster size, a result from publication **II**, is shown, in Fig. 7, for deposition with the amount of clusters ranging from one up to a total of eight clusters deposited on an initially smooth Cu (100) surface. Although the limit decreases for every cluster added, this decrease slowly subsides, and eventually there is no discernible difference between deposition of the seventh and eighth cluster. To explain this, one has to look back at Fig. 6, where the difference in potential energy decrease, or even temperature change, does not differ much between the cases of the second and third clusters, i.e. the clusters being deposited on a roughened surface.

The curvature of cluster-hillocks, remaining after previously deposited structures, is the major culprit in lessening the binding energy of an incoming cluster. However, this curvature is highly dependent on the size of the deposited clusters. If cluster size is kept constant during deposition, then the radius of the curvature of surface roughness, due to these clusters, will remain roughly the same. As initial rearrangement of a cluster landing on a smooth surface will be most substantial, as compared to the following clusters, it will be subject to the highest degree of flattening. The following cluster will be rearranged much less, leading to a lesser flattening, and eventually, when this process has continued

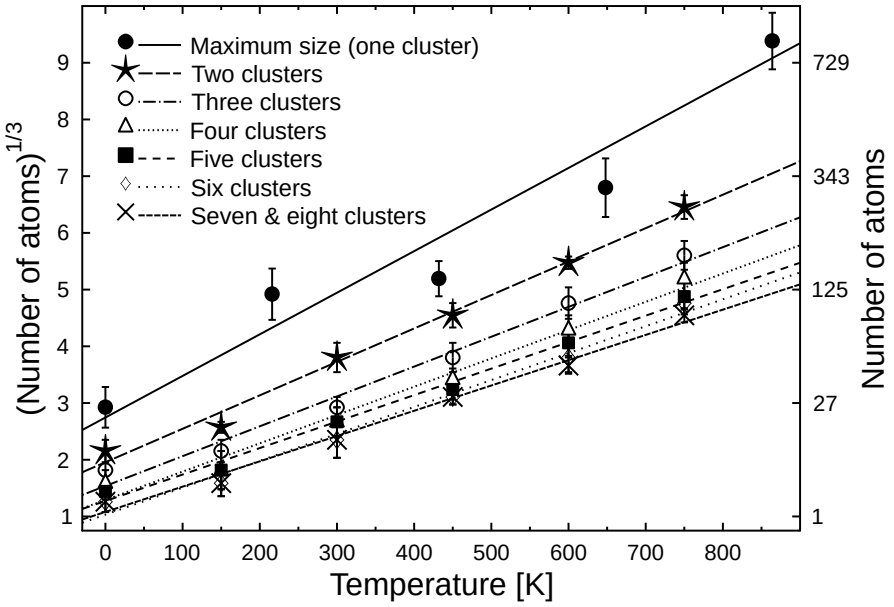

Figure 7: The maximum size of Cu clusters that achieve full contact epitaxy, when multiple clusters are deposited in sequence on an initially smooth Cu (100) substrate, as a function of the temperature of the substrate. The maximum size decreases, as the amount of clusters grows, until sizes converge at their lowest values. From publication **II**.

long enough, the structures remaining from the following clusters will adopt the same final curvature on the surface as the structure remaining from their predecessors. The end-result of this will be a finite lower limit in cluster size, for which epitaxial alignment of deposited structures should continue.

Deposition of clusters directly on top of previously deposited clusters is, however, the worst case scenario, if epitaxial alignment is desired. This is shown in the results of Fig. 8, where the degree of non-epitaxiality, for the cluster deposited second in sequence, is plotted as a function of the radial distance between the center of the first cluster-hillock and the impact point of the second cluster.

The degree of non-epitaxiality, F_{epi}, is calculated as a sum over the nearest neighbours, j, of an atom, i, as

$$F_{\mathrm{epi}} = \sum_i \min_j (\arccos |r^j_{\mathrm{Ideal}} \cdot r^i_{\mathrm{nn}}|), \tag{5}$$

where the ideal neighbour vectors are unit vectors marked r_{Ideal}, and the unit vectors for each atom to

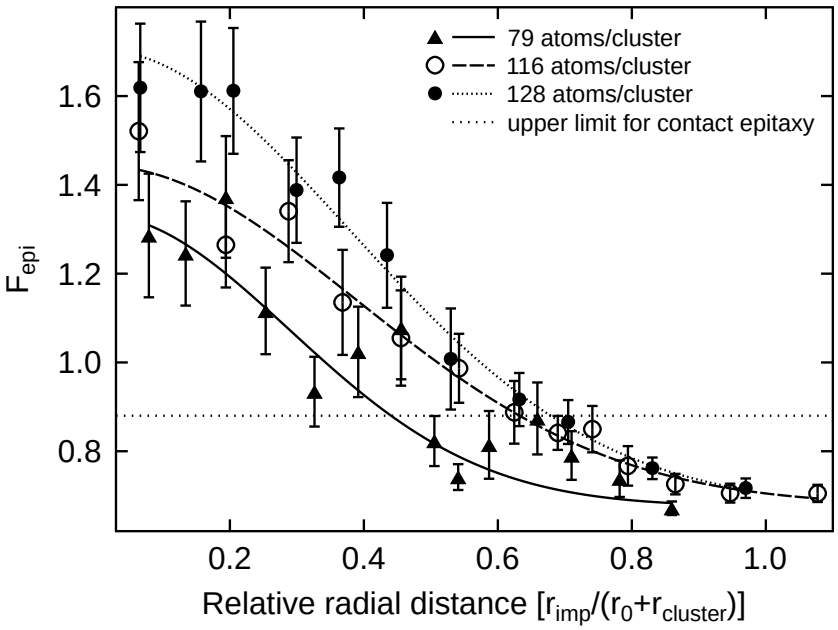

Figure 8: F_{epi}, the degree of non-epitaxiality, of the second deposited cluster, when two equisized Cu clusters of sizes 79, 116, and 128 atoms per cluster, were deposited in sequence on a 300 K substrate. This is plotted as a function of the normalized radial distance between the impact point of the second cluster and the center of the first. $F_{\mathrm{epi}} \approx 0.7$ corresponds to perfect epitaxy, whereas epitaxial configurations with higher values of F_{epi} are strained. From publication **II**.

its nearest neighbours are marked r_{nn}. For every nearest neighbour the dot product is calculated for all the ideal vectors and the vectors to the nearest neighbours, and the minimum value is added to F_{epi}. Since $\arccos(x) = 0$ when $x = 1$, this method of calculating epitaxy will be non-sensitive to surfaces (where some neighbours are completely missing).

In Fig. 8, the radial distances of impact, r_{imp}, on the x-axis are normalized with the sum of the radii of both the first, r_0, and the second cluster, r_{cluster}; hence a radial distance of more than 1.0 corresponds to a situation where the two clusters do not touch at the moment of the second cluster's impact on the surface, i.e., the second cluster is *de facto* deposited on a smooth surface. If the second cluster impacts a short distance from the center of a previous cluster, on the slope of a cluster-hillock, it will interact with a larger surface area than what is possible for impacts that occur directly on top of the hillock. Eventually, as the distance increases, incoming clusters will interact with both the cluster-hillock and the smooth substrate surface, effectively a larger surface area of interaction than for the case of a single cluster on a smooth surface.

As the distance between the impact point and the center of the previously deposited cluster increases,

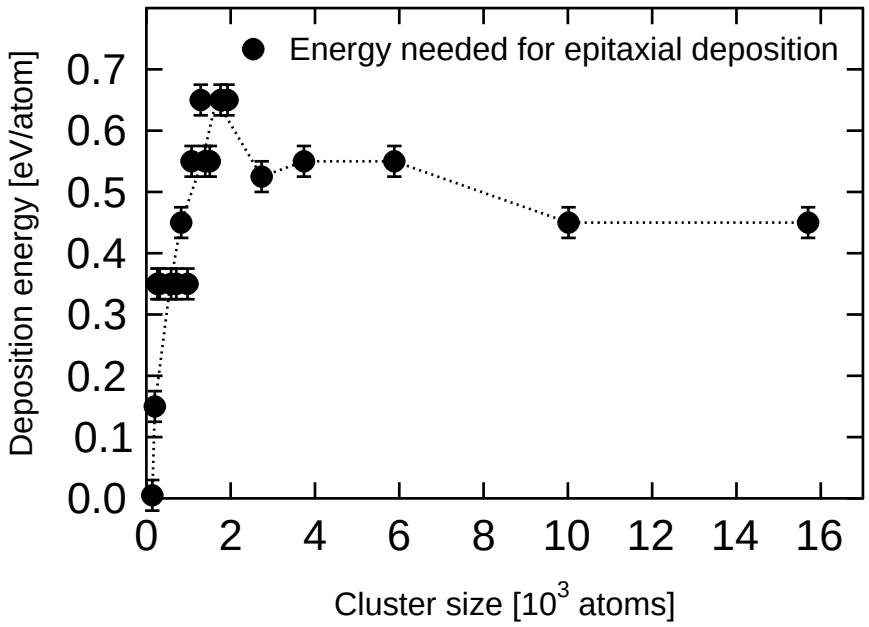

Figure 9: The minimum deposition energy per atom required for epitaxial deposition of Cu clusters, as a function of cluster size. For all sizes of clusters, if deposition occurred at favourable orientations with respect to the substrate surface, epitaxial alignment could take place at energies below the limit of minimum deposition energy required for always achieving epitaxy. The error bars do not take this into account, but merely depict the size of the chosen step in deposition energy. From publication **III**.

the likelihood of epitaxial alignment will increase. Long-time-scale effects, causing a smoothing of the cluster-hillocks, will also add a positive effect to the epitaxial deposition of multiple amounts of clusters. Deposition of clusters with sizes in a region close to the size limit for completely epitaxial deposition will produce structures that are predominately epitaxial, with the occasional smaller non-epitaxial grain.

5.1.4 Energy dependence in epitaxial deposition

A self-evident means of increasing the likelihood of an epitaxial alignment of deposited clusters – increasing the deposition energy [20], was studied in publication **III**. The temperature increase of the cluster atoms at impact, will increase if energy is added to the collision, through an increase in the deposition energy [98]. This temperature increase then results in a higher degree of initial rearrangement of the cluster atoms. Eventually, when the deposition energy is sufficiently high, all of the cluster atoms will rearrange at impact, and consequently recrystallize according to the underlying substrate.

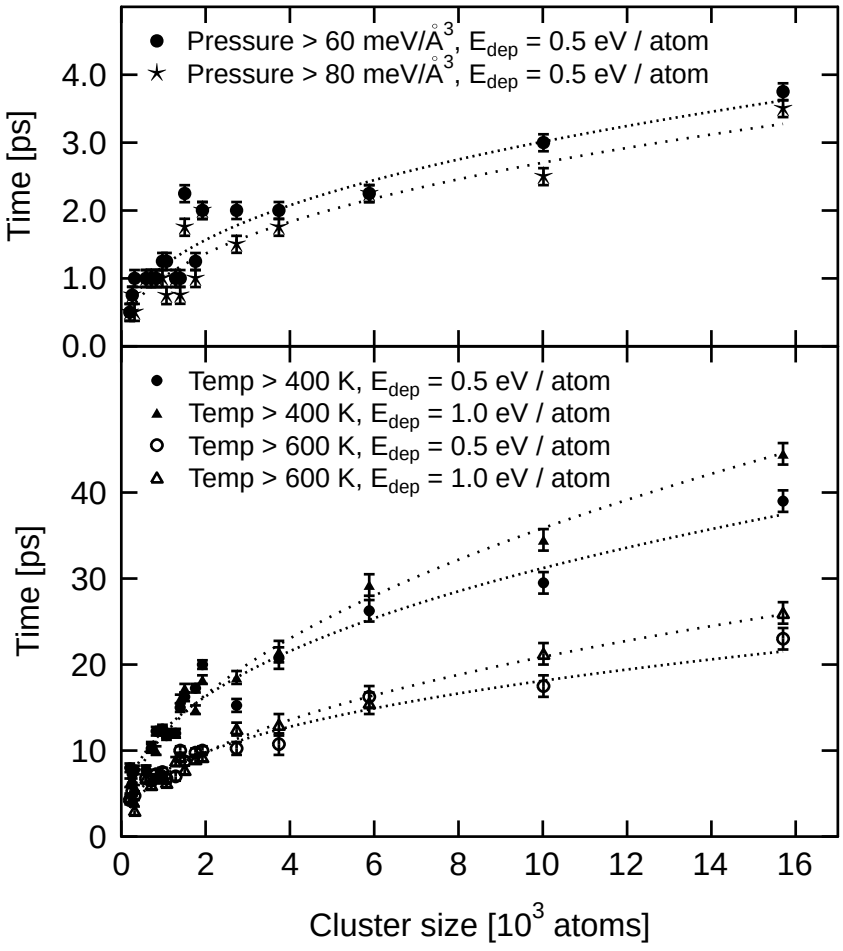

Figure 10: The time that is required for pressures and temperatures of deposited Cu clusters to decrease below values of 60 and 80 meV/Å^3, and 400 and 600 K, respectively, as a function of size, for clusters deposited with energies of 0.5 and 1.0 eV/atom on a substrate at 300 K. Increased times at higher temperatures and pressures will facilitate a greater rearrangement of cluster atoms, and therein promote the epitaxial alignment of larger clusters. From publication **III**.

In Fig. 9, the minimum deposition energy per cluster atom, required for the epitaxial deposition of various cluster sizes, is shown as a function of cluster size. For smaller cluster sizes (below 2000 atoms), there is a steep increase in the required deposition energy, as the cluster size increases. This is due to the lower ratio between the surface and volume of the clusters, which results in a lower amount of released binding energy per atom, causing a lower inherent increase in temperature upon impact, at soft landings. This steep increase continues, until a deposition energy of approximately 0.6 eV/atom is reached. This energy was proven to be sufficient for a rearrangement of the entire cluster, for all sizes of clusters studied. As this is the deposition energy per atom in the cluster, the total energy of deposition will naturally increase for larger sizes.

If cluster sizes surpass a limit of approximately 2000 atoms, the required energy for epitaxial deposition decreases. This is due to a prolonged time at which the atoms of these larger clusters are at elevated temperatures and pressures. The pressures and temperatures of all clusters increase upon impact, and although this increase is not dependent on the cluster size, the rate by which pressure diminishes and heat dissipates from the clusters is highly dependent on their size. The time that is required for pressures and temperatures to decrease below specific values, is shown in Fig. 10, as a function of cluster size.

Increased times at higher pressures and temperatures will increase the rearrangement of cluster atoms, and will also facilitate the migration of any grain boundaries that might have formed in the upper parts of the clusters. This explains why the required energy decreases slightly as clusters grow, in Fig. 9, when cluster sizes are beyond the limit of 2000 atoms. The increase in time at elevated pressures and temperatures depends logarithmically on the cluster size, and the effect will therefore result in a leveling out of the required deposition energy for epitaxial alignment, to approximately 0.45 eV/atom.

The increased time at elevated pressures also corresponds to an increase in the time of momentum transfer from the cluster to the substrate, which facilitates the formation of point defects in the substrate, even at relatively low deposition energies. For the largest clusters, interstitial formation could already be observed at an energy of 0.3 eV/atom. Although this energy is well below the formation energy of an interstitial, the high pressures involved can ease the process. The migration rate of interstitials at a temperature of 300 K is, fortunately, high enough for the rapid migration of these to the surface [99]. At lower temperatures, however, defect production could present itself as an obstacle if completely epitaxial structures are desired.

5.2 Non-epitaxial deposition

If the size of deposited clusters is above the limit presented in Section 5.1, non-epitaxial deposition will occur. The end result of such deposition will be the formation of stable grains in the upper parts of cluster-hillocks, and eventually a film containing many nano-scale grains, if deposition is continued.

Non-epitaxial deposition of smaller clusters is, however, also possible, if the strength of the interaction, between the clusters and the surface onto which they are being deposited, is lessened. One method of changing the nature of this interaction is by changing the substrate material. It is, however, good to remember that although the strength of the interaction is lessened, causing a lower binding of the cluster to the surface, other effects may incur. The interaction between clusters and their supporting surfaces must always be taken into account when depositing clusters. Exotic effects of these interactions can lead to most astounding results [35, 100–104].

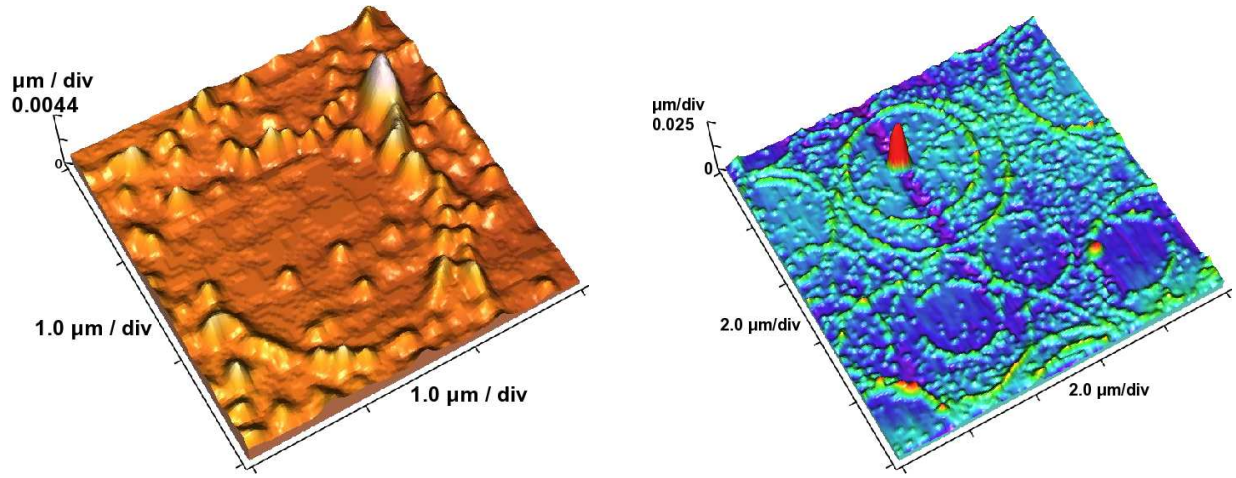

(a) (b)

Figure 11: AFM images of ring-like structures, resulting from the spontaneous organization of silica-supported metal clusters. (a) A cluster-ring with a nearly depleted center. (b) An image of a surface onto which clusters have been deposited on two separate occasions. The cluster-covered surface was allowed to stabilize in vacuum for approximately 10 hours between each deposition, which was sufficient time for the formation of the first set of rings. The appearance of concentric rings hints towards the role of specific points on the surface in arrangement of the deposited clusters. From publication **VI**.

5.2.1 Ring formation

Figure 11 shows AFM images of the self-assembled ring-like structures of copper nanoclusters supported on silica, SiO_x, surfaces that were studied in publication **VI**. The interaction between metallic clusters and the native oxide surface of a silicon substrate, differs wildly from that of a cluster on a pristine single-crystal surface of its own element [105]. The cluster-oxide interaction is rather weak, which leads to a high rate of diffusion for the clusters [101, 106, 107]. Furthermore, the silica surface, which is polar in nature, also affects the clusters by inducing dipoles in them [108–110]. These two factors contribute to a result which not even remotely comes close to epitaxial deposition.

Dipoles induced by the polar silica surface will always have the same directions, and interactions between these will therefore be repulsive. On the other hand, as clusters are easily polarized [108–112], attractive van der Waals interactions between clusters will be considerable [113, 114]. Due to a rapid diffusion of the clusters, under the influence of these two competing forces, exotic structures will have the opportunity to evolve on the surface. Clusters separated by longer distances will be pushed further from each other, whereas clusters close to each other will agglomerate. If the right conditions are available, self-assembly of ring-like structures can occur.

Proof of the validity of such an interplay of interactions was shown in publication **VI**, where molecular

dynamics simulations were used, with a code that was specifically developed for such a system. Clusters were treated as single entities with a size and mass corresponding to the 5 nm in diameter clusters of the experiment. The cluster-cluster interactions were modeled with a potential that was built up using analytical models for the dipole-dipole interaction

$$U_{d-d} = \frac{p^2}{4\pi\varepsilon_0 r^3}, \tag{6}$$

where p is the strength of the cluster dipole and r is the distance between the clusters, and a Lennard-Jones potential [115]

$$U_{vdW} = \varepsilon\left[\left(\frac{\sigma}{r}\right)^{12} - 2\left(\frac{\sigma}{r}\right)^{6}\right], \tag{7}$$

where ε is the strength of the interaction, σ the equilibrium distance and r the distance between the clusters, for the van der Waals interactions. The resulting total potential was given by

$$U_{tot} = U_{d-d} + U_{vdW}. \tag{8}$$

Similar ring-like structures were observed as a result of the relaxation of an initially random distribution of clusters.

A long-time-scale effect of these interactions, as clusters were introduced to atmospheric conditions in the process of conducting AFM analysis, was the further aggregation of the clusters, into μm-sized dots at randomly spaced intervals. These structures appeared because the surface induced dipoles diminished, due to a loss of the metallic properties, and hence polarizability, of the clusters as they were oxidized [116–118]. Similar structures could be obtained through simulations, if the strength of the van der Waals component of the cluster-cluster interaction was exaggerated.

The interactions between clusters and surfaces must always be evaluated, if thin films are to be grown by cluster deposition. There are, however, means by which effects similar to those presented in publication **VI** can be avoided. If deposition speeds are fast enough, thin films can be grown on virtually any substrate, as surface diffusion will be much slower than the rate at which new clusters impact on already deposited structures. A continued deposition and the growth of cluster islands

will immobilize them. Increasing deposition energy will also promote the growth of a more evenly distributed layer, as surface defects, induced by the high-energy density of deposition, will pin the clusters more efficiently to their impact points.

6 FILM GROWTH BY CLUSTER DEPOSITION

The deposition of single clusters on a smooth surface and surfaces roughened by the deposition itself can result in many outcomes [119, 120]. If deposition is continued even further, thin films will be grown, eventually evolving into thicker films. The morphology, and therein the physical properties, of these films will depend highly upon the conditions during deposition. If deposition energies are high enough, epitaxial films of a good quality, with good adhesion and useful mechanical properties will be the end result [121]. At lower energies, on the other hand, there remains the possibility of growing films in which clusters retain memory of their original size and structure.

6.1 The effect of cluster size

Fig. 12 shows the results of publication **IV**, where the effect of an increase in the size of deposited clusters on the density of cluster-assembled thin films, grown by low energy cluster deposition, is plotted. The density of the films decreases quite rapidly, as cluster size is increased, due the lower amount of binding energy per atom released at impact, which was discussed in the previous section.

The model of cluster heating gave an estimate of the amount of energy released, due to the loss of surface area [19], when a cluster lands on a surface, as $\Delta E = 2\gamma A$ (Eq. 2), where γ was the surface energy and 2A was the surface area lost upon adsorption. The total area lost when two clusters are sintered, can be estimated by approximating a cluster as a sphere and the surface area A by its segment, with a height h, giving $A = 2\pi rh$, where r is the radius of the cluster. In the previous model [19], for a cluster landing on a smooth surface, h was estimated to be the interaction range of the atoms, and set to be equal to one lattice constant, i.e., $h = a$. For the case of two clusters colliding, this interaction length will be shorter, due to the curvature of the clusters. If the clusters are perfectly spherical, h should take a value approximately half of what it was in the previous model, giving $h = a/2$.

The increase in temperature resulting from the release of surface energy, ΔT, is estimated, from the relation in Eq. 3, as

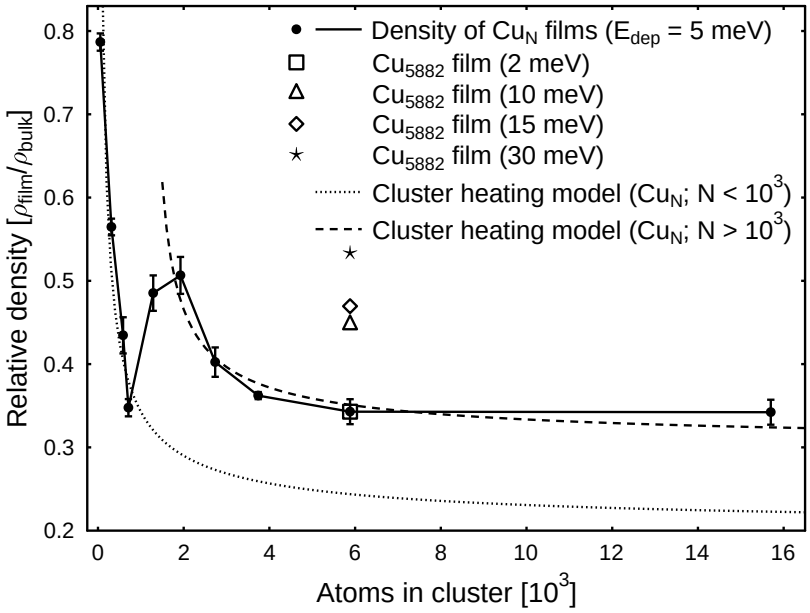

Figure 12: Density of thin films grown by low-energy deposition (5 meV/atom) of various sized clusters, as a function of the cluster size. Densities of films grown with Cu_{5882} clusters at energies of 2, 10, 15, and 30 meV/atom are also included. Densities decrease sharply, up to a threshold value in cluster size, where the results are shifted towards higher densities. This shift is due to a closer packing of clusters that no longer stick to each other as easily, when their size increases. The dotted line is a fit based on the model for cluster heating at impact, which applies to growth with clusters that have less than 1000 atoms. The dashed line shows how the density of films grown with larger clusters, above the threshold value, follows the same trend as the cluster heating model, if the model is shifted towards higher densities. From publication **IV**.

$$\frac{3}{2}Nk_B\Delta T = \frac{\gamma\pi ra}{2}, \tag{9}$$

where N is the number of atoms in the cluster, $N = \frac{16\pi r^3}{3a^3}$, and the released energy is divided by 2, due to the equipartition theorem. Combining the previous equations, and solving for the change in temperature, we get

$$\Delta T = (\frac{\pi^2}{18})^{\frac{1}{3}}\frac{\gamma a^2}{k_B}N^{-\frac{2}{3}}. \tag{10}$$

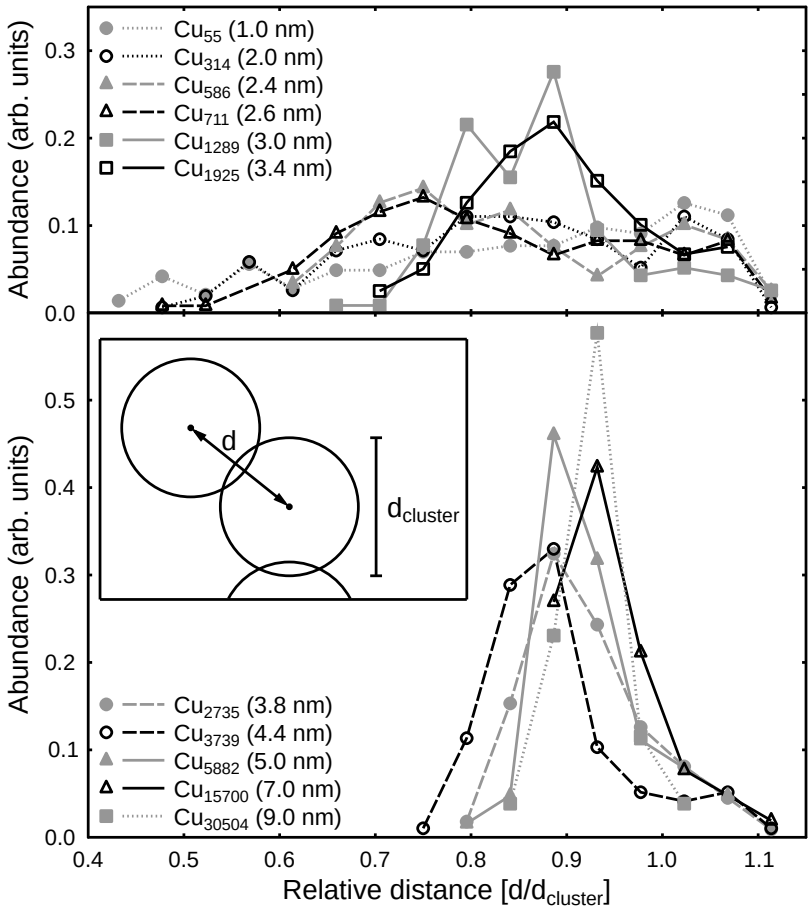

Figure 13: The distribution of relative distances between adjoining clusters in thin films assembled with various cluster sizes (cluster diameters are given in the parentheses). Deposition energies during film growth were 5 meV/atom. Distances between the centers of each cluster are normalized by twice the radius, in other words the diameter, of the clusters. The inset shows a schematic diagram of the difference between the intercluster distance, d, and the diameter of a cluster, $d_{cluster}$. From publication **IV**.

The density of a cluster-assembled thin film will increase if temperature is increased, due to an increased sintering of clusters at elevated temperatures [122], and one can therefore make the rough assumption that $\rho \propto \Delta T$, where ρ is the relative density of the film. Using this relation, equation 10 can be expressed as

$$\rho = \Lambda \frac{\gamma a^2}{k_B} N^{-\frac{2}{3}} + \rho_0, \tag{11}$$

where Λ, into which the first factor of Eq. 10 has been incorporated, and ρ_0 are fitting parameters. In

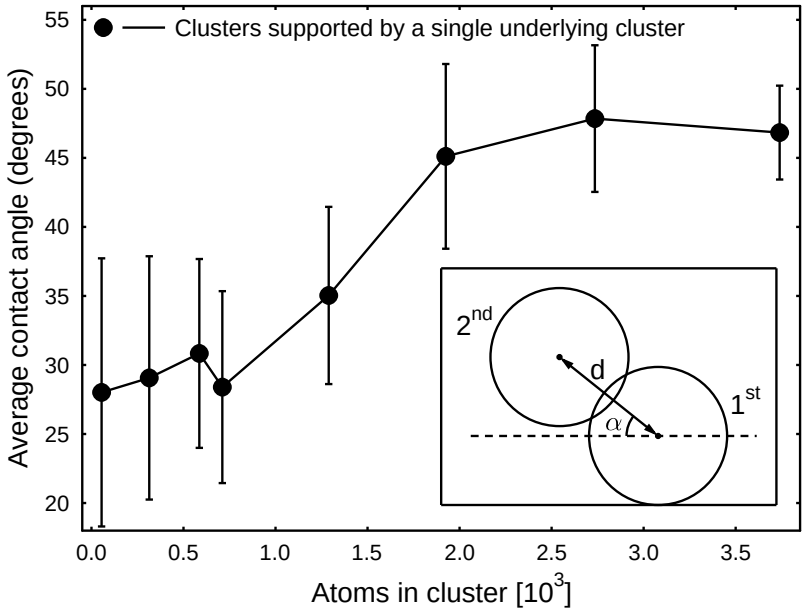

Figure 14: The average angle of contact between clusters supported by a single underlying cluster and those supporting clusters, as a function of cluster size. The contact angle is defined as such that the angle between to adjoining clusters residing in the same horizontal plane is 0°, while the contact angle for a cluster directly on top of its supporting cluster is 90°. The inset shows a schematic diagram of how this angle, α, between a previously deposited cluster (1^{st}) and a cluster deposited later (2^{nd}), is defined. From publication **IV**.

Fig. 12 the model of cluster heating has been fit to the data points of clusters with sizes below 1000 atoms, using values of $a = 3.61$ Å and $\gamma = 1.29$ J/m^2 [19], and fitting parameters $\Lambda = 0.0012$ K^{-1} and $\rho_0 = 0.2$, giving a fairly good agreement with the simulated values. The value of ρ_0, the lowest density attainable in the model, curiously enough corresponds to the relative packing density of newly fallen snow [123], a deposition process which is very similar to that of cluster deposition.

In Fig. 12 this model is presented as a dotted line, and seemingly fits well to clusters containing below approximately 1000 atoms. The trend after this limit in size follows the same trend as the heating model, except at a slight offset (the dashed line) from the original curve. At sizes above the limit, an effect of the diminished heating of the clusters at impact comes into play.

Sintering of clusters, i.e. the melting together of separate cluster at their contact points, will occur at elevated temperatures. From Fig. 13, the relative distances between clusters in films deposited at low energies (5 meV/atom), can be seen. The distributions of distances for the smaller clusters are rather uniform, with distances between the centers of adjoining clusters also being very much smaller than

the combined radii of two pristine clusters, i.e., a relative distance of 1.0. The distributions for the larger clusters, on the other hand, grow sharper and their peak values shift closer to a state where not much overlapping of clusters occurs.

Due to the diminished sintering of the larger clusters, the likelihood that two clusters, that barely touch, will stick to each other will decrease. This can be understood from the results of Fig. 14, where the average contact angle, for clusters that are supported by only a single cluster, is plotted. This angle is defined in such a way that 90° corresponds to a situation where the two clusters are directly on top of each other, while at 0° they lie side by side. When clusters with sizes above the limit of 1000 atoms impact others at a low angle, they no longer stick, but rather continue onwards, filling up the lower parts of the films, and thereby increase the average film density. The average contact angle for clusters supported by a single cluster, plotted in Fig. 14, will increase as clusters which have continued onwards will be supported by several underlying clusters.

6.2 Deposition energy

If slightly higher energies are introduced (publication **IV** and Ref. [18]), by increasing the deposition energy of the clusters, melting will increase and result in a broader distribution of the relative distances between clusters in the film. Figure 15 illustrates this for the case of films grown by deposition of Cu_{5882} clusters at different energies. From the inset in the figure, which shows film density as a function of height, it is also clear that there are no major differences in the density distribution within the films, but rather that the crucial difference, causing an increase in film density, is indeed a sintering of the clusters.

If deposition energy, on the other hand, is increased very much, significant changes will occur in the morphology of the thin films [18]. Individual clusters will be more closely packed, as energy increases, but above a certain limit, the melting of clusters at impact will be too severe, and the nanocrystalline grain structure of the films will start to disappear. This is a phenomena closely related to the minimum energy required for epitaxial deposition of single clusters on smooth surfaces, which was presented in Section 5.1.4.

As energy increases, the density of the films will increase, which can be seen in Fig. 16(a), where the density of Cu_{586} cluster-assembled thin films is plotted for different deposition energies and amounts of deposited clusters. An energy increase produces films with a density profile approaching that of the bulk throughout the entire film, in Fig. 16(b), even at a deposition energy as low as 300 meV/atom. The minimum energy required for epitaxial deposition of clusters, however, lies fairly close to these

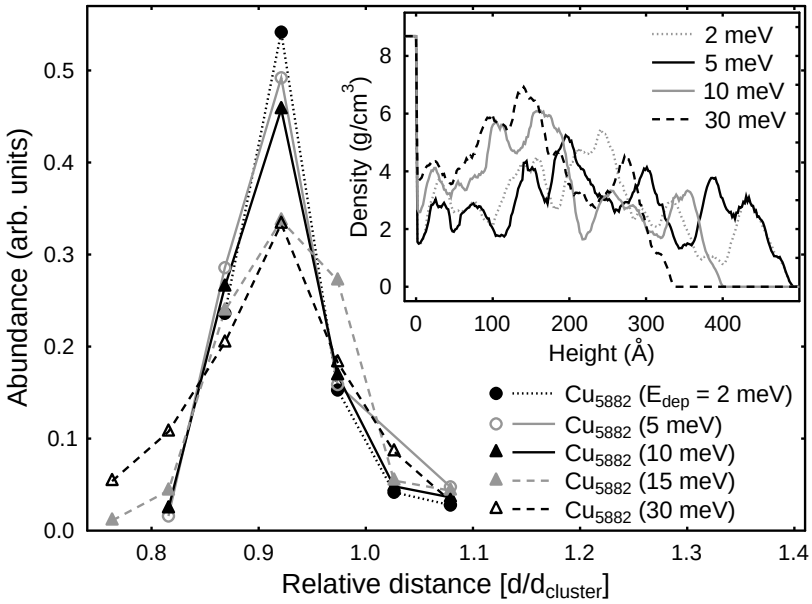

Figure 15: The distribution of relative distances between adjoining clusters in films grown by deposition of Cu_{5882} clusters at various energies. A clear flattening of the distribution can be observed, as deposition energies are increased. The inset shows density profiles for these films, where average density is plotted against distance from the surface of the substrate. From publication **IV**.

values, for clusters of this size. Deposition at this energy will therefore result in films that are very nearly epitaxial.

At deposition energies high enough for the growth of dense thin films, every single cluster will melt entirely at impact, and subsequently recrystallize, adopting an orientation which is aligned with the underlying structure. On a single crystal substrate, the grown film will therefore itself be single-crystalline. Nanocrystallinity and high density can not be achieved, merely by increasing deposition energies.

The average relative film densities for all of the thin films, shown in Fig. 16(a), are well below that of bulk copper. This is mainly due to surface roughness. As can be seen from the density profiles in Fig. 16(b), bulk densities are achieved for the lower parts of all of the films that contain 50 clusters and were deposited at energies higher than 300 meV/atom. Only at the top-most surface of the films does this density decrease. Surface roughness should not be included when the average densities are evaluated, as it merely stems from a local variation in the level of the surface, and is not a true indication of a lower density. The effect of surface roughness is the main reason for a lowering of the average densities of the films containing fewer than 50 clusters, in Fig. 16(a). This lowering can be

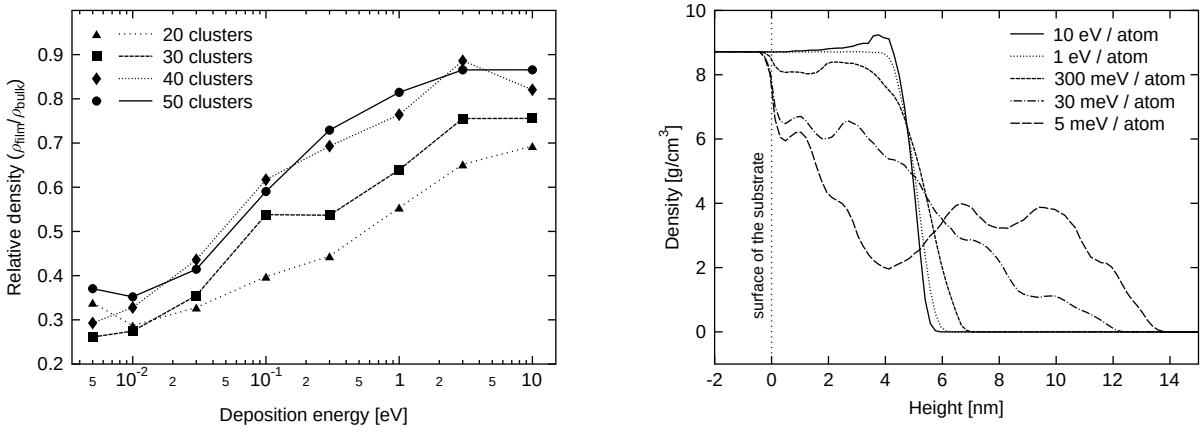

(a) (b)

Figure 16: (a) The average relative density of Cu_{586} cluster-assembled thin films as a function of deposition energy. The densities of films, as compared to that of bulk copper, are shown for different amounts of deposited clusters. (b) Thin film density profiles after deposition of 50 Cu_{586} clusters at various deposition energies. The graph shows the average film density as a function of the height above the substrate. Nanocrystallinity is preserved in films that are grown with deposition energies below 300 meV/atom. These are, however, very porous throughout their entire thicknesses and will exhibit poor mechanical qualities. From [18].

attributed to an increase in the relative thickness of the surface layer, as the total thickness of the films is lower, when fewer clusters have been deposited.

Increased deposition energies will produce denser thin films with better mechanical durability and adhesion. The nanocrystallinity of these films, however, will not be preserved, as the clusters melt upon impact, and recrystallize according to the already existing crystalline directions of the underlying substrate. Low-energy deposition of clusters is the only possibly route, if nano-scale properties, in the resulting thin films, are desirable. Other means of improving the mechanical properties of the thin films must therefore be introduced.

7 MODIFICATION OF CLUSTER-ASSEMBLED THIN FILMS

If thin films with properties resembling those of free clusters, i.e., nanocrystalline films, are to be grown, low-energy deposition of clusters is a prerequisite. The mechanical properties of such films are however too poor [42], and post-deposition modification of the films must occur if they are to be

of use in applications. The major flaws of these films are a very poor durability and thermal stability, as they are simply too porous. A densification of these films is therefore necessary.

Several methods of producing nanocrystalline thin films by densification of nanocrystalline powders already exist. These methods rely on elevated pressures, where the powders are compressed by a large force onto the surface of the substrate, or on high temperatures, as clusters are sintered together by increased thermal activity [122, 124, 125]. The drawbacks of these methods are the harshness towards the substrate, excluding the use of many interesting substrate materials, and the severe grain growth that occurs during these processes, leading to thin films with much larger grains than the size of the original nanoparticles in the powders. An alternative method of cluster-assembled thin film densification was initially studied (in publication **VI**) using MD simulations, and later confirmed as viable through the experimental results presented in Section 7.1.1.

7.1 Densification by ion irradiation

Heavy ion irradiation is the key to a modification of cluster-assembled thin films, without irreversibly altering their nanocrystalline properties. Heavy ion irradiation induces amorphization and viscous flow in crystalline semiconductors and ceramics [126–128]. Although similar irradiation of close-packed structures commonly does more harm than good [129], through the creation of numerous defects [130, 131] and therein brittleness, the irradiation of porous structures could be beneficial. If initially under-dense structures are irradiated with heavy ions, local melting and a viscous flow of atoms will result in the filling of voids, and hence a densification of the structure. If recrystallization of molten regions occurs fast enough, and according to the local structure of individual clusters, nanocrystallinity is preserved within the films.

MD simulations of the irradiation of cluster-assembled thin films was performed using Xe and Au ions at various energies and fluences. The results of these simulations are shown in Fig. 17, where the average increase in thin film density, for irradiation with various energies, is shown as a function of fluence. Results for density calculations, where both the surface has been included and excluded, are shown.

Differences in the rates of densification, for the different ions and energies of irradiation, can be explained by considering the range and energy deposition of the respective ions in copper, at their different energies. The range of Xe in copper is higher than that of Au, which results in a slightly larger deposition of energy at the lower layers of the film. At higher energies the ranges of both Xe and Au ions are such that energy is deposited throughout the entire films. At these energies, 15 keV and above, the amount of deposited energy per ion is higher for Au, resulting in a faster densification

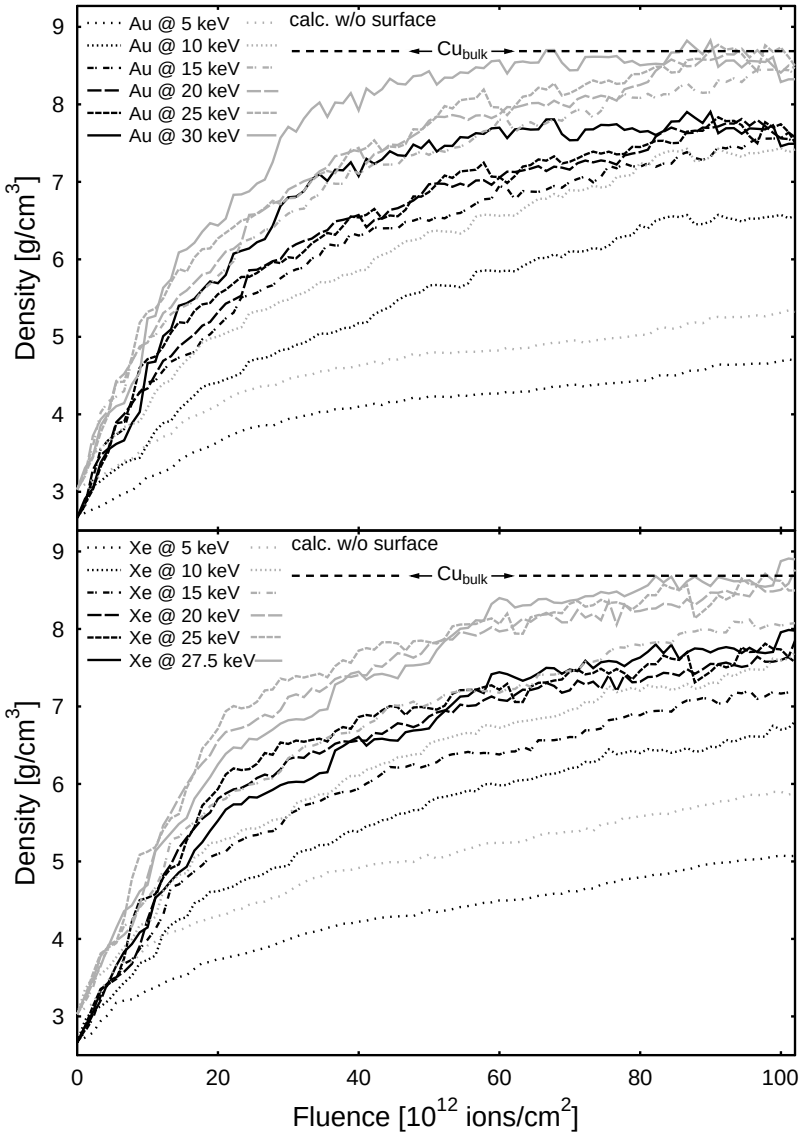

Figure 17: Average density of Cu_{711} cluster-assembled thin films after irradiation with Xe and Au ions at various energies, as a function of fluence. Due to the substrate size, every ion impact represents an approximate fluence of 1.11×10^{12} ions/cm^2, hence a fluence of 100×10^{12} ions/cm^2 is approximately achieved with 90 ion impacts. The increase in density is initially a very rapid event, but subsides as the density of the films grows. The average density of the entire thin films, visualized using black lines, is compared to their calculated densities when the topmost 15 % of the thin film is removed, shown as grey lines, in order to lessen the effect of surface roughness. Once the topmost layers of the film are removed from the density calculations, it can clearly be seen that the density of the thin films approaches that of bulk copper, even at the fairly low fluences of approximately 60×10^{12} ions/cm^2. From publication **V**.

process for this ion. The differences in rate of densification between Xe and Au is, however, only slight for these energies.

Once again, surface roughness comes into play in the density calculations in these results. For Xe ions at energies above 20 keV, a sharp kink in the densification curves can be seen at a fluence of approximately 20×10^{12} ions/cm^2. Initially there is a rapid increase in density at fluences below 20×10^{12} ions/cm^2, which corresponds to a densification of the whole film. After this the rate of densification decreases at higher fluences, as voids within the film have been filled and only surface smoothing takes place. The surface layer is, however, initially rather thick and only at a fluence of 80×10^{12} ions/cm^2 does the under-dense surface layer shrink to below 15 % of the film thickness, which is the thickness of the layer removed, when excluding the surface from calculations on the film density. A surface layer of only 15 % of the film thickness was, however, chosen in order to allow for a larger part of the atoms of the film ($\sim$ 92 %) to be included in the density calculations.

7.1.1 Experimental results

The experimental results of thin film densification with ion irradiation can be seen in Fig. 18, which shows an AFM image of the interface region between an irradiated and as-deposited Cu cluster-assembled thin film. Initial film thickness, measured to be approximately 200 nm, was decreased by approximately 40 nm after irradiation with Ar ions at an energy of 150 keV and a fluence of 10^{15} ions/cm^2. The cluster-assembled thin films were partially irradiated, while keeping the non-irradiated part covered by a mask for the duration of the heavy ion bombardment. This was done in order to achieve a difference in height between the irradiated and as-deposited film. The border between the irradiated and as-deposited parts of the film was then analysed by AFM, and was found to be sharp enough for the use in analysis of the densification, which occurred during the irradiation process.

If initial film densities are know, assuming the same amount of atoms per unit area remains in the densified films, the new density can be calculated from the decrease in film height, or the height of the step between the irradiated and the non-irradiated parts of the film. The relative increase in density of the films, $\Delta\rho/\rho_{\text{dep}}$, where $\Delta\rho = \rho_{\text{irrad}} - \rho_{\text{dep}}$, and ρ_{dep} and ρ_{dep} are the densities before and after irradiation, can be calculated as

$$\frac{\Delta\rho}{\rho_{\text{dep}}} = \frac{\rho_{\text{irrad}} - \rho_{\text{dep}}}{\rho_{\text{dep}}}. \tag{12}$$

Further, $\rho_{\text{irrad}} = \sigma m/\tau_{\text{irrad}}$ and $\rho_{\text{dep}} = \sigma m/\tau_{\text{dep}}$, where τ_{dep} and τ_{irrad} are the thicknesses of the respective films, which are separated by a step height of $h_{\text{step}} = \tau_{\text{dep}} - \tau_{\text{irrad}}$. σ is the areal density of atoms and m is the mass of a single atom of that element. Combining these equations then gives a final relative increase in density as

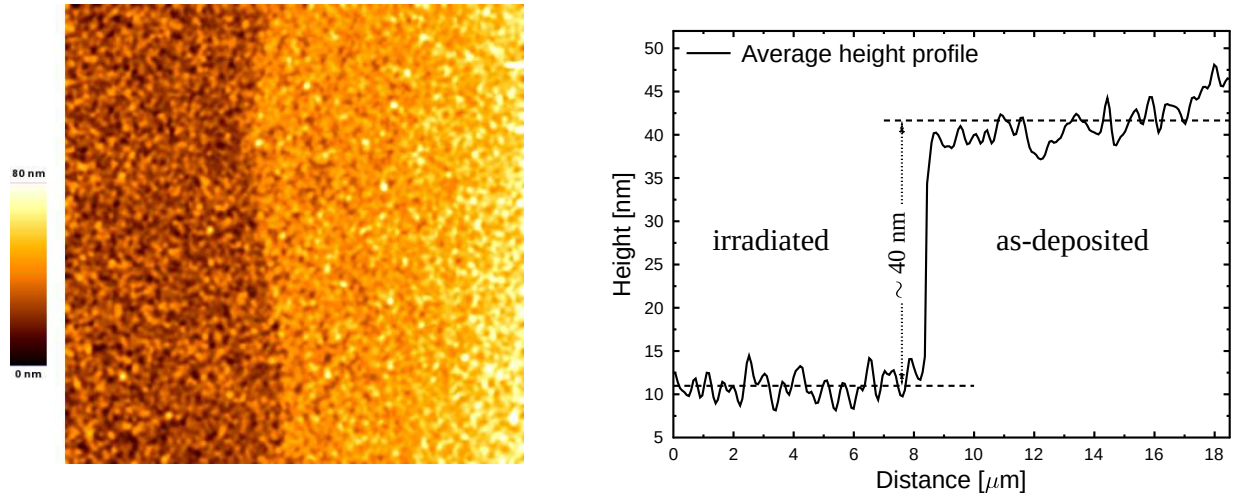

(a) (b)

Figure 18: (a) An AFM image (scan size 20 μm) showing the interface between an as-deposited Cu cluster-assembled thin film (grown on an oxidised Si substrate) and a part of the film that has been irradiated with Ar ions at an energy of 150 keV and a fluence of 10^{15} ions/cm^2. (b) The average height profile of the interface region, as measured by AFM. The irradiated (darker) area of the surface is approximately 40 nm lower than the as-deposited (lighter) film, indicating a denser packing of the irradiated film.

$$\frac{\Delta\rho}{\rho_{\mathrm{dep}}} = \frac{\tau_{\mathrm{dep}}}{\tau_{\mathrm{dep}} - h_{\mathrm{step}}} - 1. \tag{13}$$

A decrease of approximately 40 nm, for a film that originally had a thickness of 200 nm, therefore gives an increase in film density of $\sim 25\%$, according to these calculations.

Cluster-assembled thin films were also irradiated with a focused ion beam at 30 keV, and the changes in film morphology were monitored by *in situ* scanning electron microscopy (SEM). In Fig. 19(a), the as-deposited thin film, consisting of columnar structures of deposited clusters, is shown. The size of the clusters used in this experiment was larger than the corresponding clusters of the simulations, with cluster diameters approaching 20 nm (instead of the 3 nm in diameter clusters of the films deposited with MD).

The very much larger size of the experimentally deposited clusters, coupled together with only a slightly deeper range for Ga ions as compared to Xe or Au, resulted in the majority of the structural changes taking place at the surface layers of the thin film. The height of the irradiated part of the thin film has not decreased, i.e. the average density of the film will be the same, however, as can be seen

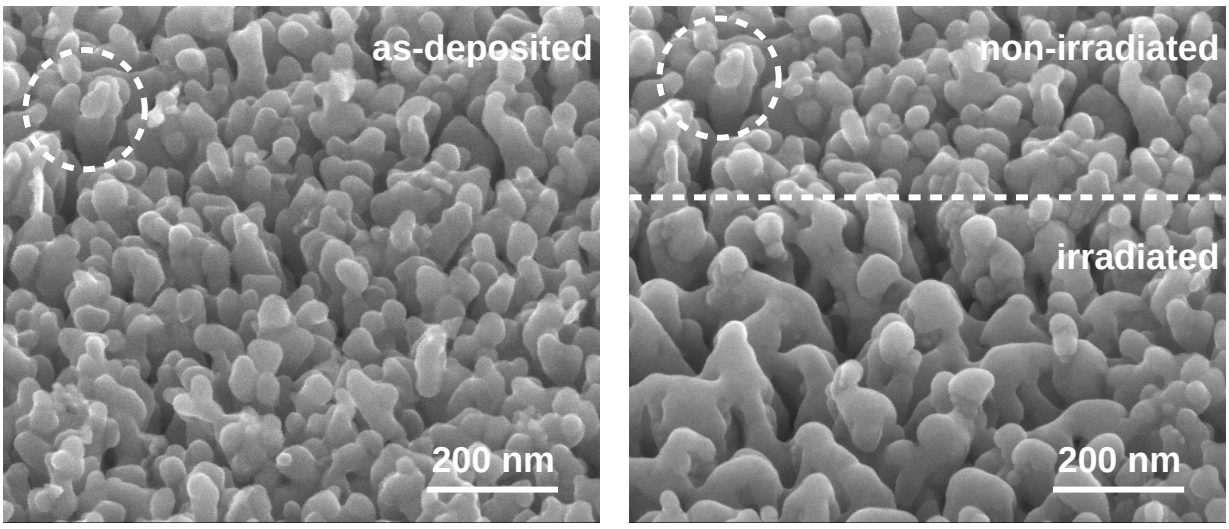

Figure 19: SEM images of (a) an as-deposited Cu cluster film, and (b) the same film after the lower part (below the dashed line) has been irradiated by a 30 keV focused Ga^+ ion beam. The penetration depth of the Ga ions is not large enough to cause a densification of the entire thin film, but a clear difference can be seen, as surface layers of the film have been affected by the impinging ions. The same position has been encircled in both images, in order to ease the comparison between them.

from the SEM image in Fig. 19(b), significant changes to the structures which have been irradiated have occurred.

The same position has been encircled in both images of Figure 19, in order to ease the comparison between the irradiated film, both before and after irradiation. One can clearly see that smaller features have merged together, giving clear evidence for the densifying effect of ion irradiation. With ion energies tweaked for a deeper range into the thin film layer, a densification of the whole film is possible. Ion fluences must, however, be rather low if nano-scale grains within the film are to be conserved, a feat which is very difficult when irradiating with focused ion beams. The use of more flexible accelerators, with a wider variety of ion species, is therefore recommended.

7.1.2 The stability of grains during irradiation

The stability of grains within the film, during irradiation, was studied in the molecular dynamics simulations of publication **V**. Grains were observed to grow slightly, but not with a critical severity. Fig. 20 shows the remaining grain boundaries within two thin films irradiated at different energies, where atoms within stacking faults and twin boundaries are shown as slightly larger than atoms within a FCC configuration.

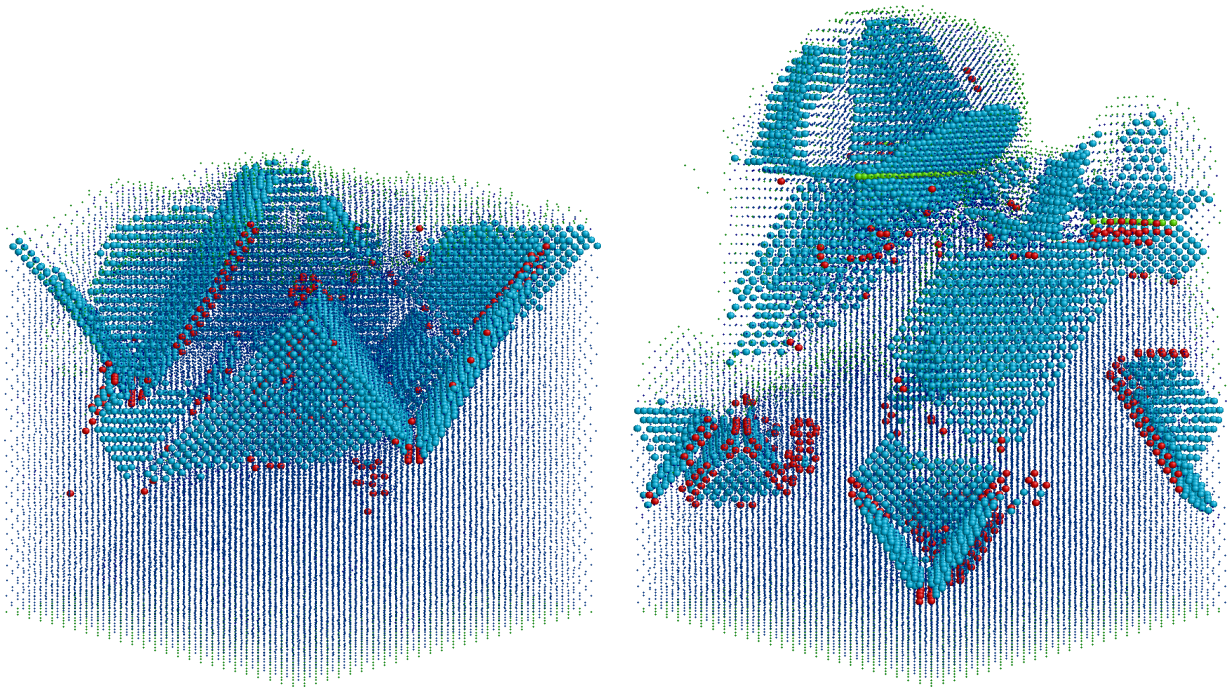

(a) (b)

Figure 20: Snapshots showing dislocations and grain boundaries present in a film after (a) irradiation with Au ions at an energy of 30 keV and a fluence of approximately 60×10^{12} ions/cm^2, and (b) after irradiation with Au ions at an energy of 5 keV and a fluence of 100×10^{12} ions/cm^2. Atoms within stacking faults and twin boundaries are shown as slightly larger than atoms within a FCC configuration. From publication **V**.

As the decisive mechanism causing densification is the melting and recrystallization of local regions within the thin films, it is only natural to presume that grain growth will also occur. Grain growth has, likewise, been reported in several theoretical and experimental papers focused on changes in morphology during the irradiation of nanocrystalline samples [132–135].

As the thin films are compressed during the densification process, single clusters will sinter with others, and therein adopt a different orientation. Because melting occurs locally, and recrystallization is such a fast process, several crystal orientations will, however, remain within the film, as grains with different orientations will simultaneously grow in several locations. If a global melting had occurred, recrystallization would proceed according to some predominant orientation, thereby resulting in the growth of very much larger grains.

The existence of several different crystal orientations, as seen in the snapshots in Fig. 20, confirms the fact that the cluster-assembled films retain nanocrystallinity throughout the densification process. Although the grain size has undoubtedly grown, these are still rather small. It is, however, clear that

their final size will be very much dependent on the original size of the deposited clusters and the energy at which the films are irradiated.

7.1.3 Sputtering

The loss of atoms from the thin films, due to a sputtering of atoms during irradiation, was out of necessity studied in publication **V**. An erosion of the thin films by sputtering of atoms, could be a major concern with the use of heavy ion irradiation for the modification of their mechanical properties. At ion energies and fluences, as low as the ones used in the simulations, the sputtering rate of copper is, however, not very high [136].

Sputtering yields from the thin films could be split into two different categories, namely the yields from films with densities below a threshold of 6.0 g/cm^3, and yields from films that were denser than this. At densities below this value, larger aggregates could sometimes be sputtered from the films, as large parts of still ascertainable individual clusters were detached from the films. At higher densities the likelihood for such events was minimal. This effect also seemed to be energy dependent, as sputtering yields for the under-dense films increased as ion energy increased, but only up to a specific point. Once ion energies, and therefore ion ranges, were too high, sputtering yields decreased. This can be explained by the fact that atoms sputtered from lower parts of under-dense films were captured by the upper parts of those films.

Sputtering yields were also higher for the heavier ions. For all ion species the yields were, however, low enough to allow for less than 3 % of the films to be sputtered away during irradiation. Sputtering yields from thin films with density above 6.0 g/cm^3 were well within the range of experimental values [136].

7.2 Alloyed thin films

Another interesting application of thin film growth, through the low-energy deposition of clusters, exists. Due to the highly non-equilibrium conditions of cluster condensation, the aggregation of clusters composed of virtually any stoichiometry is possible [137]. This even includes the aggregation of materials that, under normal conditions, are immiscible. If thin films could be grown by deposition of, i.e., bi-metallic clusters of any combination of metals, new exotic alloyed thin films, with exciting applicability, could be the end-result [138]. As with any films grown by low-energy cluster deposition, these films would, however, have to be densified before they could withstand extreme physical conditions.

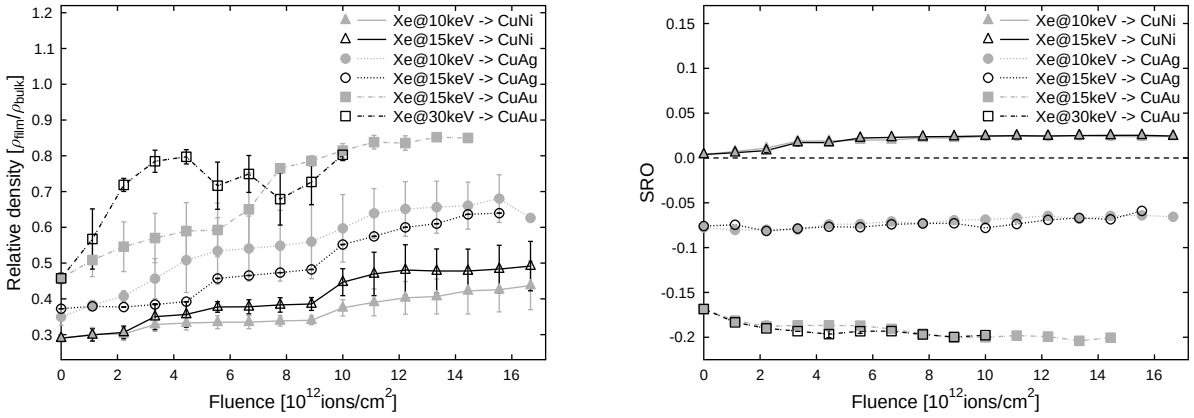

(a) (b)

Figure 21: (a) The average relative density of CuAu, CuAg, and CuNi bimetallic thin films as a function of fluence, after irradiation with Xe ions at various energies. (b) The short-range order parameter (SRO) for the same bimetallic thin films as a function of fluence. Density of the thin films can be increased by irradiation with heavy ions, without inducing significant segregation of the different metal species.

For the densification of alloyed thin films to be successful, another criterion must be fulfilled. Grain growth is not necessarily an issue, but a segregation of the elemental components must be prevented for the films to be true alloys [139]. Methods that involve the elevation of temperature cannot be used, as the diffusion of atoms within the alloy lattice increases heavily for even the slightest increase in temperature. Densification by heavy ion irradiation can be a viable option, as ion impacts result in only a local increase in temperature, and this increase is very short-lived. If recrystallization is rapid enough, not to allow for the diffusion of atoms, the order, or rather disorder, of the alloy will be preserved.

The growth of alloyed thin films was simulated, by deposition of several of the bi-metallic clusters CuAu, CuAg, and CuNi at a temperature of 300 K [21]. Each cluster contained 711 atoms, distributed approximately evenly over the two elemental components of the clusters. The elements were all distributed randomly in the clusters. Deposition was performed in a fashion similar to that of pure elemental clusters, and afterwards irradiation of these films with heavy ions was likewise performed in the same manner as that described in Section 7.1. The results of this irradiation is shown in Fig. 21, where the density of the bi-metallic films, and the short-range order parameter, indicating if segregation of the elements occurs, are plotted as a function of fluence.

The short-range order parameter (SRO), defined as

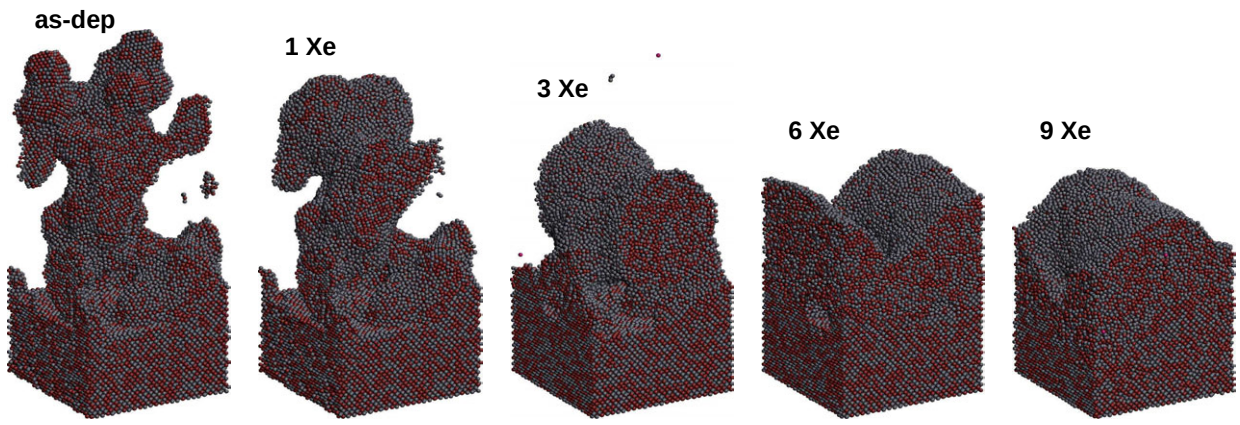

Figure 22: Snapshots of a CuAg thin film, both as-deposited, and after impacts of increasing amounts of Xe ions at an energy of 15 keV per ion. With as little as nine impacts, corresponding to a fluence of approximately 10^{13} ions/cm^2, the structure of the thin film has seemingly approached that of a bulk alloy.

$$\mathrm{SRO} = 1 - \frac{n_{\mathrm{AB}}/n_{\mathrm{B}}}{c_{\mathrm{A}}} \tag{14}$$

where $n_{\mathrm{AB}}/n_{\mathrm{B}}$ is the probability that an atom of type A is nearest neighbour to an atom of type B, and c_{A} is the concentration of species A, gives a measure of how segregated or ordered a lattice of a binary alloy is. If the two components of the lattice are completely segregated, SRO should adopt a value of 1, whereas a completely ordered alloy, will have $\mathrm{SRO} = -1$. A value of 0 will be the result if the elements of the lattice are at entirely random positions [140, 141].

As can be seen from the results, density can be increased without a severe segregation of the elements in the films. The increase in density of the thin films may, however, not appear to be significant enough, if only viewed through the results presented in Fig. 21. It must, nonetheless, be remembered that the effect of surface roughness in a lowering of the average density of the thin films is remarkable. Fig. 22 shows snapshots of a CuAg thin film, both as-deposited and after the impacts of a growing amount of Xe ions at 15 keV/ion. Even at the fairly low irradiation energy of 15 keV, the morphology of the thin film has approached a condition close to that of the bulk substrate, after as little as nine ion impacts. With the surface area of this particular film, nine impacts are approximately equivalent to a fluence of 10^{13} ions/cm^2.

8 CONCLUSIONS

Using a combination of molecular dynamics simulations and the experimental deposition and analysis of nanoclusters, cluster-surface interactions, as well as growth mechanisms of cluster-assembled thin films, have been studied. The results show how clusters can be used for the growth of nanostructured thin films with tailored properties, by variations in simple deposition parameters, such as cluster size and deposition energy. This thesis also shows the importance of understanding the interactions between nanometer-sized objects and their supporting surfaces, when dealing with nano-scale systems.

Using molecular dynamics simulations, it was shown that there exists an upper limit in cluster size, below which clusters will align epitaxially on a smooth surface of the same material. This limit is both dependent on temperature and deposition energy, as well as on the rate at which clusters are deposited. If clusters, with sizes below this limit, are deposited, the resulting structures that grow will be epitaxial, and cluster-assembled thin films will have a high density. If cluster sizes above this limit are used, structured thin films, such as nanocrystalline films, can be grown.

By tweaking the size of the deposited clusters, and the energy at which they were deposited, thin films with a wide variety of morphologies can be grown. As deposition energies are increased, the densities of the resulting films will likewise increase by a logarithmic dependence. On the other hand, if cluster size is decreased, independent of deposition energy, film density will also increase. The use of small clusters, or high energies, will produce epitaxial films, with good adhesion and high durability, whereas larger clusters, deposited at low energies, will result in nanocrystalline films.

Nanocrystalline thin films, grown by low-energy cluster deposition, tend to be porous and have a poor mechanical durability. If they are to be used in any real applications, these films must be modified by some means after deposition. Modification of cluster-assembled thin films, by irradiation with heavy ions, proved to be a successful method of improving the mechanical properties of thin films, most notably their densities, without irreversibly harming their nanocrystalline structure. This was initially predicted by simulations, and later verified through experiments.

Already a relatively low fluence of heavy ion impacts is sufficient for the densification of porous cluster-assembled thin films towards near-bulk densities. Local melting, coupled with a viscous flow of the molten regions, and recrystallization, according to the already present crystalline orientations of the deposited clusters, was shown to be the mechanisms behind this densification. As the molten regions were very small, and recrystallization was a rapid event, the grain sizes within the nanocrystalline films did not suffer from a severe growth.

The growth and modification of alloyed thin films, even consisting of immiscible materials, was shown to be possible with low-energy cluster deposition. The subsequent modification of these films, by heavy ion irradiation, improved film properties without causing a large segregation of the separate atom species. The growth of thin films, composed of virtually any stoichiometry, was shown to be feasible with these methods.

The possible applications of nanocluster deposition rely heavily on the careful choice of deposition parameters. If the interactions between deposited clusters and their supporting surfaces are sufficiently well understood, a multitude of practical outcomes from cluster deposition will be available. In our search for novel functional structures, nanoclusters may be the building blocks of the future.

ACKNOWLEDGMENTS

I wish to thank Prof. Juhani Keinonen, the head of the Department of Physics, for the opportunity to conduct research on cluster deposition, and for his kind advice and help during this work. Many thanks are also due to the current and former heads of the Accelerator Laboratory, Prof. Jyrki Räisänen and Doc. Eero Rauhala, for providing the facilities of the laboratory to my disposal.

I am most grateful to my supervisor Prof. Kai Nordlund, for introducing me to the field of materials physics, and for later pushing me into the exciting world of nanoscience. Thank you, for your never-ending encouragement and your zealous approach toward the life of a scientist – you set an example for all of us.

I am also dearly indebted to my colleagues and friends at the laboratory, especially Tommi, Caro, Nicke, and Jani. All the long days at work have almost been a pleasure when spent in your company. Thank you for making my life, both in and outside of the laboratory, so much more enjoyable.

The warmest thanks are due to my family, friends, and relatives for their inexhaustible support throughout the years.

Most importantly, I wish to thank Matilda. Without you, I doubt I would ever have had the strength or the proper reason to finish this thesis. You have shown me the real meaning of life.

Financial support from the Academy of Finland and the Alfred Kordelin Foundation is gratefully acknowledged.

Helsinki, June 26, 2009
Kristoffer Meinander

References

1. R. P. Feynman, *There's plenty of room at the bottom*, Engineering and Science (California Institute of Technology, Pasadena, CA, USA) **Vol. XXIII**, 22 (Feb. 1960).

2. G. Binnig, H. Rohrer, C. Gerber, and E. Weibel, *Surface Studies by Scanning Tunneling Microscopy*, Phys. Rev. Lett. **49**, 57 (1982).

3. K. Meinander, in *Reflexer*, edited by K. Meinander (Fysikersamfundet i Finland – Suomen Fyysikkojen Seura, Helsingfors, 2008), Vol. 10, pp. 8–13.

4. G. Padeletti and P. Fermo, *How the masters in Umbria, Italy, generated and used nanoparticles in art fabrication during the Renaissance period*, Appl. Phys. A **76**, 515 (2003).

5. M. Josè-Yacamán, L. Rendón, J. Arenas, and M. C. S. Puche, *Maya Blue Paint: An Ancient Nanostructured Material*, Science **273**, 223 (1996).

6. D. J. Barber and I. C. Freestone, *An investigation of the origin of the colour of the Lycurgus Cup by analytical transmission electron microscopy*, Archaeometry **32**, 33 (1990).

7. G. L. Hornyak, C. J. Patrissi, E. B. Oberhauser, C. R. Martin, J.-C. Valmalette, L. Lemaire, J. Dutta, and H. Hofmann, *Effective medium theory characterization of Au/Ag nanoalloy-porous alumina composites*, Nanostruct. Mater. **9**, 571 (1997).

8. C. G. Granqvist and R. A. Buhrman, *Ultrafine metal particles*, J. Appl. Phys. **47**, 2200 (1976).

9. R. A. Buhrman and C. G. Granqvist, *Log-normal size distributions from magnetization measurements on small superconducting Al particles*, J. Appl. Phys. **47**, 2220 (1976).

10. K. Sattler, J. Mühlbach, and E. Recknagel, *Generation of metal clusters containing from 2 to 500 atoms*, Phys. Rev. Lett. **45**, 821 (1980).

11. T. G. Dietz, M. A. Duncan, D. E. Powers, and R. E. Smalley, *Laser production of supersonic metal cluster beams*, J. Chem. Phys. **74**, 6511 (1981).

12. K. Wegner, P. Piseri, H. Vahedi Tafreshi, and P. Milani, *Cluster beam deposition: a tool for nanoscale science and technology*, J. Phys. D: Appl. Phys. **39**, R439 (2006).

13. F. Baletto and R. Ferrando, *Structural properties of nanoclusters: Energetic, thermodynamic, and kinetic effects*, Rev. Mod. Phys. **77**, 371 (2005).

14. A. Perez, P. Melinon, V. Dupuis, P. Jensen, B. Prevel, J. Tuaillon, L. Bardotti, C. Martet, M. Treilleux, M. Broyer, M. Pellarin, J. Vaille, B. Palpant, and J. Lerme, *Cluster assembled materials: a novel class of nanostructured solids with original structures and properties*, J. Phys. D: Appl. Phys. **30**, 709 (1997).

15. R. W. Siegel, *Cluster-assembled nanophase materials*, Annu. Rev. Mater. Sci. **21**, 559 (1991).

16. P. Jensen and N. Combe, *Understanding the grwoth of nanocluster films*, Comp. Mater. Sci. **24**, 78 (2002).

17. K. Meinander, J. Frantz, K. Nordlund, and J. Keinonen, *Upper size limit of complete contact epitaxy*, Thin Solid Films **425**, 297 (2003).

18. K. Meinander, T. Clauß, and K. Nordlund, in *Growth, Modification, and Analysis by Ion Beams at the Nanoscale*, Vol. 908E of *MRS Symposium Proceedings*, edited by W. Jiang (MRS, Warrendale, PA, USA, 2006), pp. 0908–OO14–20.1.

19. T. T. Järvi, A. Kuronen, K. Meinander, K. Nordlund, and K. Albe, *Contact epitaxy by deposition of Cu, Ag, Au, Pt, and Ni nanoclusters on (100) surfaces: Size limits and mechanisms*, Phys. Rev. B **75**, 115422 (2007).

20. K. Nordlund, T. T. Järvi, K. Meinander, and J. Samela, *Cluster ion-solid interactions from meV to MeV energies*, Appl. Phys. A **91**, 561 (2008), invited paper.

21. K. Meinander and K. Nordlund, (2009), to be published.

22. M. Brack, *The physics of simple metal clusters: self-consistent jellium model and semiclassical approaches*, Rev. Mod. Phys **65**, 677 (1993).

23. W. A. de Heer, *The physics of simple metal clusters: experimental aspects and simple models*, Rev. Mod. Phys **65**, 611 (1993).

24. P. Milani and S. Iannotta, *Cluster Beam Synthesis of Nanostructured Materials*, *Springer series in cluster physics* (Springer-Verlag, Berlin, 1999).

25. D. Herschbach, *Chemical physics: Molecular clouds, clusters, and corrals*, Rev. Mod. Phys. **71**, 411 (1999).

26. G. Apai, J. F. Hamilton, J. Stohr, and A. Thompson, *Extended X-ray-absorption fine structure of small Cu and Ni clusters: Binding-energy and Bond-length changes with cluster size*, Phys. Rev. Lett. **43**, 165 (1979).

27. M. Schmidt, R. Kusche, T. Hippler, J. Donges, W. Kronmüller, B. von Issendorff, and H. Haberland, *Negative heat capacity for a cluster of 147 sodium atoms*, Phys. Rev. Lett. **86**, 1191 (2001).

28. R. Kusche, T. Hippler, M. Schmidt, B. von Issendorff, and H. Haberland, *Melting of free sodium clusters*, Eur. Phys. J. D **9**, 1 (1999).

29. H. Lei, *Melting of free copper clusters*, J. Phys. Cond. Matt. **13**, 3023 (2001).

30. C. L. Cleveland, W. D. Luedtke, and U. Landman, *Melting of gold clusters*, Phys. Rev. B **60**, 5065 (1999).

31. E. E. Zhurkin and M. Hou, *Structural and thermodynamic properties of elemental and bimetallic nanoclusters: an atomic scale study*, J. Phys.: Condens. Matter **12**, 6735 (2000).

32. W. D. Knight, K. Clemenger, W. de Heer, W. Saunders, M. Y. Chou, and M. L. Cohen, *Electronic shell structure and abundances of sodium clusters*, Phys. Rev. Lett. **52**, 2141 (1984).

33. R. Schlipper, R. Kusche, B. v. Issendorff, and H. Haberland, *Thermal emission of electrons from highly excited sodium clusters*, Appl. Phys. A **72**, 255 (2001).

34. M. Ghaly and R. S. Averback, in *Beam Solid Interactions: Fundamentals and Applications Symposium*, Vol. 279 of *Mat. Res. Soc. Symp. Proc.*, edited by M. Nastasi, L. R. Harriott, N. Herbots, and R. S. Averback (Mat. Res. Soc., Pennsylvania, 1993), pp. 17–22.

35. P. Jensen, *Growth of nanostructures by cluster deposition: Experiments and simple models*, Rev. Mod. Phys. **71**, 1695 (1999).

36. I. Yamada, *Low-energy cluster ion beam modification of surfaces*, Nucl. Instr. and Meth. in Phys. Res. B **148**, 1 (1999).

37. N. Toyoda, N. Hagiwara, J. Matsuo, and I. Yamada, *Surface smoothing mechanism of gas cluster ion beams*, Nucl. Instr. and Meth. in Phys. Res. B **161-163**, 980 (2000).

38. M. Moseler, O. Rattunde, J. Nordiek, and H. Haberland, *On the origin of surface smoothing by energetic cluster impact: Molecular dynamics simulation and mesoscopic modeling*, Nucl. Instr. and Meth. in Phys. Res. B **164-165**, 522 (2000).

39. Z. Insepov and I. Yamada, *Surface modification with ionised cluster beams: Modelling*, Nucl. Instr. and Meth. in Phys. Res. B **148**, 121 (1999).

40. I. Yamada, J. Matsuo, Z. Insepov, T. Aoki, T. Seki, and N. Toyoda, *Nano-processing with gas cluster ion beams*, Nucl. Instr. and Meth. in Phys. Res. B **164-165**, 944 (2000).

41. Y. Qiang, Y. Thurner, T. Reiners, O. Rattunde, and H. Haberland, *Hard coatings (TiN, $Ti_xAl_{1-x}N$) deposited at room temperature by energetic cluster impact*, Surface and Coatings Technology **100-101**, 27 (1998).

42. H. Haberland, Z. Insepov, M. Karrais, M. Mall, M. Moseler, and Y. Thurner, *Thin films from energetic cluster impact: experiment and molecular dynamics simulation*, Nucl. Instr. and Meth. in Phys. Res. B **80/81**, 1320 (1993).

43. H. Haberland, Z. Insepov, and M. Moseler, *Molecular-dynamics simulation of thin-film growth by energetic cluster impact*, Phys. Rev. B **51**, 11061 (1995).

44. H. Haberland, M. Moseler, Y. Qiang, O. Rattunde, T. Reiners, and Y. Thurner, *Energetic cluster impact (ECI): A new method for thin-film formation*, Surf. Rev. and Lett. **3**, 887 (1996).

45. S. P. R. E. Palmer and H.-G. Boyen, *Nanostructured surfaces from size-selected clusters*, Nature Materials **2**, 443 (2003).

46. K. S. Kumar, H. V. Swygenhoven, and S. Suresh, *Mechanical behaviour of nanocrystalline metals and alloys*, Acta Materialia **51**, 5743 (2003).

47. M. A. Laguna, V. Paillard, B. Kohn, M. Ehbrecht, F. Huisken, G. Ledoux, R. Papoular, and H. Hofmeister, *Optical properties of nanocrystalline silicon thin films produced by size-selected cluster beam deposition*, J. Lumin. **80**, 223 (1999).

48. A. Harjunmaa, J. Tarus, K. Nordlund, and J. Keinonen, *MD simulations of the cluster beam deposition of porous Ge*, Eur. Phys. J. D **43**, 165 (2007).

49. I. Yamada, J. Matsuo, N. Toyoda, and A. Kirkpatrick, *Materials processing by gas cluster ion beams*, Mat. Sci. Eng. R **34**, 231 (2001).

50. H. Haberland, M. Karrais, M. Mall, and Y. Thurner, *Thin films from energetic cluster impact: A feasibility study*, J. Vac. Sci. Technol. A **10**, 3266 (1992).

51. S.-Y. Jeon, N.-J. Seong, J.-K. Ahn, H.-W. Lee, and S.-G. Yoon, *Nanocluster deposition for oxide thin film growth at near room temperature*, Nanotechnology **19**, 435305 (2008).

52. I. Yamada, *Novel materials processing and applications by gas cluster ion beams*, Eur. Phys. J. D **9**, 55 (1999).

53. M. P. Allen and D. J. Tildesley, *Computer Simulation of Liquids* (Oxford University, Oxford, England, 1989).

54. B. J. Alder and T. E. Wainwright, in *Molecular Dynamics by Electronic Computers*, *Proc. Intern. Symposium on Transport Processes in Statistical Mechanics* (Wiley Interscience, New York, 1957), p. 97.

55. B. J. Alder and T. E. Wainwright, *Studies in Molecular Dynamics. I. General Method*, J. of Chem. Phys. **31**, 459 (1959).

56. K. Nordlund, *Molecular dynamics simulation of ion ranges in the 1 – 100 keV energy range*, Comput. Mater. Sci. **3**, 448 (1995).

57. A. Caro and M. Victoria, *Ion-electron interaction in molecular-dynamics cascades*, Phys. Rev. A (General Physics) **40**, 2287 (1989).

58. M. W. Finnis, P. Agnew, and A. J. E. Foreman, *Thermal excitation of electrons in energetic displacement cascades*, Phys. Rev. B **44**, 567 (1991).

59. K. Nordlund, M. Ghaly, R. S. Averback, M. Caturla, T. Diaz de la Rubia, and J. Tarus, *Defect production in collision cascades in elemental semiconductors and FCC metals*, Phys. Rev. B **57**, 7556 (1998).

60. M. Ghaly, K. Nordlund, and R. S. Averback, *Molecular dynamics investigations of surface damage produced by keV self-bombardment of solids*, Phil. Mag. A **79**, 795 (1999).

61. M. S. Daw and M. I. Baskes, *Embedded-atom method: Derivation and application to impurities, surfaces, and other defects in metals*, Phys. Rev. B **29**, 6443 (1984).

62. S. M. Foiles, *Application of the embedded-atom method to liquid transition metals*, Phys. Rev. B **32**, 3409 (1985).

63. S. M. Foiles, M. I. Baskes, and M. S. Daw, *Embedded-atom-method functions for the fcc metals Cu, Ag, Au, Ni, Pd, Pt, and their alloys*, Phys. Rev. B **33**, 7983 (1986).

64. J. F. Ziegler, J. P. Biersack, and U. Littmark, *The Stopping and Range of Ions in Matter* (Pergamon, New York, 1985).

65. G. J. Ackland and V. Vitek, *Many-body potentials and atomic-scale relaxations in noble-metal alloys*, Phys. Rev. B **41**, 10324 (1990).

66. H. Deng and D. J. Bacon, *Simulation of point defects and threshold displacements in pure Cu and a dilute Cu-Au alloy*, Phys. Rev. B **48**, 10022 (1993).

67. H. J. C. Berendsen, J. P. M. Postma, W. F. van Gunsteren, A. DiNola, and J. R. Haak, *Molecular dynamics with coupling to external bath*, J. Chem. Phys. **81**, 3684 (1984).

68. J. E. Hearn and R. L. Johnston, *Modeling calcium and strontium clusters with many-body potentials*, J. Chem. Phys. **107**, 4674 (1997).

69. P. A. Montano, G. K. Shenoy, E. Alp, W. Schulze, and J. Urban, *Structure of copper microclusters isolated in solid argon*, Phys. Rev. Lett. **56**, 2076 (1986).

70. L. Vitos, A. V. Ruban, H. L. Skriver, and J. Kollár, *The surface energy of metals*, Surface Science **411**, 186 (1998).

71. J. Urban, H. Sack-Kongehl, K. Weiss, I. Lisiecki, and M.-P. Pileni, *Structures of clusters*, Cryst. Res. Technol. **35**, 731 (2000).

72. S. Valkealahti and M. Manninen, *Instability of cuboctahedral copper clusters*, Phys. Rev. B **45**, 9459 (1992).

73. H. Haberland, M. Karrais, and M. Mall, *A new type of cluster and cluster ion source*, Z. Phys. D **20**, 413 (1991).

74. T. Aaltonen, M. Ritala, Y.-L. Tung, Y. Chi, K. Arstila, K. Meinander, and M. Leskelä, *Atomic Layer Deposition of Noble Metals: Exploration of the Low Limit of the Deposition Temperature*, J. Mater. Res. **19**, 3353 (2004).

75. M. T. Räisänen, P. de Almeida, K. Meinander, M. Kemell, I. Mutikainen, M. Leskelä, and T. Repo, *Cobalt salen functionalised polycrystalline gold surfaces*, Thin Solid Films **516**, 2948 (2008).

76. M. V. Lindén, K. Meinander, A. Helle, G. Yohannes, M.-L. Riekkola, S. J. Butcher, T. Viitala, and S. K. Wiedmer, *Characterization of phosphatidylcholine / PEG-lipid aggregates and their use as coatings and carriers in CE*, Electrophoresis **29**, 852 (2008).

77. L. D'Ulivo, J. Chen, K. Meinander, K. Öörni, P. T. Kovanen, and M.-L. Riekkola, *In situ delipidation of LDL in electrochromatographic capillaries yields apoB-100 coated surfaces for interaction studies*, Analytical Biochemistry **383**, 38 (2008).

78. R. Howland and L. Benetar, *A practical guide to scanning probe microscopy* (Park Scientific Instruments, Sunnyvale, CA, USA, 1996).

79. H. L. Lei, Q. Hou, and M. Hou, *Effect of cluster size on Cu/Au (111) epitaxy*, J. Phys.: Condens. Matter **12**, 8387 (2000).

80. G. Fuchs, P. Melinon, F. Santos Aires, M. Treilleux, B. Cabaud, and A. Hoareau, *Cluster-beam deposition of thin metallic antimony films: Cluster-size and deposition-rate effects*, Phys. Rev. B **44**, 3926 (1991).

81. F. J. Palacios, M. P. Iñiguez, M. J. López, and J. A. Alonso, *Molecular-dynamics study of the structural rearrangements of Cu and Au clusters softly deposited on a Cu(001) surface*, Phys. Rev. B **60**, 2908 (1999).

82. F. J. Resende and B. V. Costa, *Molecular dynamics study of the copper cluster depsition on a Cu(100) surface*, Surf. Sci. **481**, 54 (2001).

83. M. Yeadon, M. Ghaly, J. C. Yang, R. S. Averback, and J. M. Gibson, *"Contact Epitaxy" observed in supported nanoparticles*, Appl. Phys. Lett. **73**, 3208 (1998).

84. M. Yeadon, J. C. Yang, M. Ghaly, K. Nordlund, R. S. Averback, and J. M. Gibson, *Zooming in on clusters: novel behavior of supported metal nanocrystals*, J. Elect. Microsc. **48**, 1075 (1999), suppl. S.

85. M. Yeadon, J. C. Yang, M. Ghaly, R. S. Averback, and J. M. Gibson, *Novel interactions of supported clusters: contact epitaxy*, Mater. Sci. Eng. 76 (1999).

86. A. V. Granato, *Interstitialcy Model for Condensed Matter States of Face-Centered-Cubic Metals*, Phys. Rev. Lett. **68**, 974 (1992).

87. K. Nordlund and R. S. Averback, in *Defect and Diffusion in Metals - Annual Retrospective 2000*, edited by D. J. Fisher (Scitec Publications, Zürich, Switzerland, 2000).

88. R. W. Cahn, *Melting from within*, Nature **413**, 582 (2001).

89. M. Forsblom and G. Grimvall, *How superheated crystals melt*, Nature Materials **4**, 388 (2005).

90. F. Delogu, *On the relationship between the mechanical and the thermal instabilities of crystalline lattices*, Mat. Sci. Eng. A **403**, 48 (2005).

91. M. Yeadon, J. C. Yang, R. S. Averback, J. W. Bullard, D. L. Olynick, and J. M. Gibson, *In-situ observations of classical grain growth mechanisms during sintering of copper nanoparticles on (001) copper.*, Appl. Phys. Lett. **71**, 1631 (1997).

92. M. Yeadon, J. C. Yang, R. S. Averback, J. W. Bullard, and J. M. Gibson, *Sintering of silver and copper nanoparticles on (001) copper observed by in-situ ultrahigh vacuum transmission electron microscopy*, Nanostruct. Mater. **10**, 731 (1998).

93. S.-C. Lee, B. D. Yu, D.-Y. Kim, and N. M. Hwang, *Effects of cluster size and substrate temperature on the homoepitaxial deposition of Au clusters*, J. Cryst. Growth **242**, 463 (2002).

94. M. Hou, *A molecular dynamics evidence for enhanced cluster beam epitaxy*, Nucl. Instr. and Meth. in Phys. Res. B **135**, 501 (1998).

95. Y. Ashkenazy, R. S. Averback, and K. Albe, *Nanocluster rotation on Pt surfaces: Twist boundaries*, Phys. Rev. B **64**, 205409 (2001).

96. J. Frantz, M. Rusanen, K. Nordlund, and I. T. Koponen, *Evolution of Cu nanoclusters on Cu (100)*, J. Phys.: Condens. Matter **16**, 2995 (2004).

97. G. Palasantzas, S. A. Koch, and J. T. M. D. Hosson, *Growth front roughening of room-temperature deposited copper nanocluster films*, Appl. Phys. lett. **81**, 1089 (2002).

98. S.-C. Lee, N. M. Hwang, B. D. Yu, and D.-Y. Kim, *Molecular dynamics simulation on the deposition behavior of nanometer-sized Au clusters on a Au (001) surface*, J. Crystal Growth **223**, 311 (2001).

99. J. Steigman, W. Shockley, and F. C. Nix, *The self-diffusion of copper*, Phys. Rev. **56**, 13 (1939).

100. Z. Tang, N. A. Kotov, and M. Giersig, *Spontaneous organization of single CdTe nanoparticles into luminescent nanowires*, Science **297**, 237 (2002).

101. L. Bardotti, P. Jensen, A. Hoareau, M. Treilleux, and B. Cabaud, *Experimental Observation of Fast Diffusion of Large Antimony Clusters on Graphite Surfaces*, Phys. Rev. Lett. **74**, 4694 (1995).

102. K. V. P. M. Shafi, I. Felner, Y. Mastai, and A. Gedanken, *Olympic ring formation from newly prepared barium hexaferrite nanoparticle suspension*, J. Phys. Chem. B **103**, 3358 (1999).

103. P. C. Ohara, J. R. Heath, and W. M. Gelbart, *Self-assembly of submicrometer rings of particles from solutions of nanoparticles*, Angew. Chem. Int. Ed. Engl. **36**, 1077 (1997).

104. B. K. Min, A. K. Santra, and D. W. Goodman, *Understanding silica-supported metal catalysts: Pd / silica as a case study*, Catal. Today **85**, 113 (2003).

105. E. R. Weber, *Transition metals in silicon*, Appl. Phys. A **30**, 1 (1983).

106. P. Deltour, J.-L. Barrat, and P. Jensen, *Fast Diffusion of a Lennard-Jones Cluster on a Crystalline Surface*, Phys. Rev. Lett. **78**, 4597 (1997).

107. L. Bardotti, P. Jensen, A. Hoareau, M. Treilleux, B. Cabaud, A. Perez, and F. C. S. Aires, *Diffusion and aggregation of large antimony and gold clusters deposited on graphite*, Surf. Sci. **367**, 276 (1996).

108. W. D. Knight, K. Clemenger, W. A. de Heer, and W. A. Saunders, *Polarizability of alkali clusters*, Phys. Rev. B **31**, 2539 (1985).

109. M. B. Knickelbein, *Electric dipole polarizabilities of copper clusters*, J. Chem. Phys. **120**, 10450 (2004).

110. V. V. Kresin and C. Guet, *Long-range polarization interactions of metal clusters*, Phil. Mag. B **79**, 1401 (1999).

111. P. Calaminici, A. M. Köster, A. Vela, and K. Jug, *Comparison of static polarizabilities of Cu_n, Na_n, and Li_n ($n \leq 9$) clusters*, J. Chem. Phys. **113**, 2199 (2000).

112. P. Calaminici, *Polarizability of Fe_n ($n \leq 4$) clusters: an all-electron density functional study*, Chem. Phys. Lett. **387**, 253 (2004).

113. L. Serra and F. Garcias, *van der Waals attractions between simple metal clusters: Core effects using realistic pseudopotentials*, Phys. Rev. B **53**, 7006 (1996).

114. J.-P. Sonnenberg and E. Schmidt, *Numerical calculations of London – van der Waals adhesion force distributions for different superquadratic shaped particles*, Part. Part. Syst. Charact. **22**, 45 (2005).

115. J. E. Lennard-Jones, *On the determination of molecular fields. II. From the equation of state of a gas*, Proc. Roy. Soc. London Ser. A **106**, 463 (1924).

116. A. H. Sørensen, A. Kühle, L. T. Hansen, H. Busch, L. J. Christiansen, J. Mikkelsen, N. Herholdt-Rasmussen, K. A. Mørch, and J. Bohr, *Halo-like structures studied by atomic force microscopy*, Z. Phys. D **40**, 509 (1997).

117. J. Urban, H. Sack-Kongehl, and K. Weiss, *HREM studies of the structure and the oxidation process of copper clusters created by inert gas aggregation*, Z. Phys. D **36**, 73 (1996).

118. F. J. Williams, N. Malikova, and R. M. Lambert, *An AFM study of the genesis and sintering in hydrogen of a realistic Cu/amorphous silica planar model catalyst*, Catal. Lett. **90**, 177 (2003).

119. C. L. Kelchner and A. E. DePristo, *Molecular dynamics simulation of low energy cluster deposition during diffusion-limited thin film growth*, Nanostruct. Mat. **8**, 253 (1997).

120. Q. Hou, M. Hou, L. Bardotti, B. Prével, P. Mélinon, and A. Perez, *Deposition of AuN clusters on Au(111) surfaces. I. Atomic-scale modeling*, Phys. Rev. B **62**, 2825 (2000).

121. J. Kraft, O. Rattunde, O. Rusu, A. Häfele, and H. haberland, *Thin films from fast clusters: golden TiN layers on a room temperature substrate*, Surf. Coat. Technol. **158-159**, 131 (2002).

122. P. Moskovkin and M. Hou, *Thermal evolution of cluster assembled Ni_3Al materials modelled at the atomic scale*, Eur. Phys.J. D **27**, 231 (2003).

123. B. A. Power, *Relationship between density of newly fallen snow and form of snow crystals*, Nature **193**, 1171 (1962).

124. M. Hou and P. Moskovkin, *Thermal properties of thin and thick Ni_3Al cluster assembled layers: an atomic scale simulation study*, Appl. Surf. Sci. **226**, 161 (2004).

125. S. R. Bhattacharyya, D. Datta, I. Shyjumon, B. M. Smirnov, T. K. Chini, D. Ghose, and R. Hippler, *Growth and melting of silicon supported silver nanocluster films*, J. Phys. D: Appl. Phys. **42**, 035306 (2009).

126. M. Ghaly and R. S. Averback, *Effect of Viscous Flow on Ion damage near Solid Surfaces*, Phys. Rev. Lett. **72**, 364 (1994).

127. C. A. Volkert, *Stress and plastic flow in silicon during amorphization by ion bombardment*, J. Appl. Phys. **70**, 3521 (1991).

128. C. M. Lopatin, T. L. Alford, V. B. Pizziconi, M. Kuan, and T. Laursen, *Ion -beam densification of hydroxyapatite thin films*, Nucl. Instr. and Meth. in Phys. Res. B **145**, 522 (1998).

129. M. Nastasi, J. Mayer, and J. Hirvonen, *Ion-Solid Interactions - Fundamentals and Applications* (Cambridge University Press, Cambridge, Great Britain, 1996).

130. M. Samaras, P. M. Derlet, H. V. Swygenhoven, and M. Victoria, *SIA activity during irradiation of nanocrystalline Ni*, J. Nucl. Mater. **323**, 213 (2003).

131. M. Samaras, P. M. Derlet, H. V. Swygenhoven, and M. Victoria, *Atomic scale modelling of the primary damage state of irradiated fcc and bcc nanocrystalline metals*, J. Nucl. Mater. **351**, 47 (2006).

132. W. Voegeli, K. Albe, and H. Hahn, *Simulation of grain growth in nanocrystalline nickel induced by ion irradiation*, Nucl. Instr. Meth. Phys. Res. B **202**, 230 (2003).

133. S. G. Mayr and R. S. Averback, *Evolution of morphology in nanocrystalline thin films during ion irradiation*, Phys. Rev. B **68**, 075419 (2003).

134. N. Nita, R. Schaeublin, M. Victoria, and R. Z. Valiev, *Effects of irradiation on the microstructure and mechanical properties of nanostructured materials*, Philos Mag. **85**, 723 (2005).

135. D. Kaoumi, A. T. Motta, and R. C. Birtcher, *Grain grwoth in Zr-Fe thin films during in situ ion irradiation in a TEM*, Nucl. Instr. and Meth. in Phys. Res. B **242**, 490 (2006).

136. A. Oliva-Florio, R. A. Baragiola, M. M. Jakas, E. V. Alonso, and J. Ferrón, *Noble-gas ion sputtering yield of gold and copper: Dependence on the energy and angle of incidence of the projectiles*, Phys. Rev. B **35**, 2198 (1987).

137. B. Pauwels, G. V. Tendeloo, E. Zhurkin, M.Hou, G. Verschoren, L. T. Kuhn, W. Bouwen, and P. Lievens, *Transmission electron microscopy and Monte Carlo simulations of ordering in Au-Cu clusters produced in a laser vaporization source*, Phys. Rev. B **63**, 165406 (2001).

138. G. H. Jóhannesson, T. Bligaard, A. V. Ruban, H. L. Skriver, K. W. Jacobsen, and J. K. Nørskov, *Combined Electronic Structure and Evolutionary Search Approach to Materials Design*, Phys. Rev. Lett. **88**, 255506 (2002).

139. M. Hou, V. S. Kharlamov, and E. E. Zhurkin, *Atomic-scale modeling of cluster-assembled Ni_xAl_{1-x} thin films*, Phys. Rev. B **66**, 195408 (2002).

140. J. M. Cowley, *An Approximate Theory of Order in Alloys*, Phys. Rev. **77**, 669 (1950).

141. M. Plischke and D. Mattis, *Short-Range Versus Long-Range Order in a Model Binary Alloy*, Phys. Rev. Lett. **27**, 42 (1971).